The macrophage – hepatocyte iron communication during mycobacterial infection

Henrique Benjamin Martins Ramos
Master's Degree in Biochemistry
Faculty of Sciences of University of Porto and Abel Salazar Biomedical Sciences Institute of University of Porto
2023/2024

The macrophage – hepatocyte iron communication during mycobacterial infection

Henrique Benjamin Martins Ramos

Dissertation carried out as part of the Master's Degree in Biochemistry
2023/2024

Supervisor
Ana Carolina Moreira, PhD, i3S – Instituto de Investigação e Inovação em Saúde, Universidade do Porto; ICBAS – Instituto de Ciências Biomédicas Abel Salazar, Universidade do Porto

Co-supervisor
Tânia Martins da Silva, PhD, i3S – Instituto de Investigação e Inovação em Saúde, Universidade do Porto; ICBAS – Instituto de Ciências Biomédicas Abel Salazar, Universidade do Porto

Acknowledgements

Ao aproximar-me do final desta etapa tão importante gostava de agradecer a todas as pessoas que, direta ou indiretamente, contribuíram para este trabalho e que me acompanharam ao longo do meu percurso.

Antes de mais tenho de agradecer à minha orientadora, a Carolina, por toda a sua disponibilidade e acompanhamento, não só durante a tese, mas durante os últimos 3 anos. Quero agradecer-lhe toda a ajuda durante o meu primeiro contacto com o mundo da investigação. Agradeço também à Tânia por todos os conselhos e ensinamentos.

Gostava também de agradecer à Professora Salomé a oportunidade de poder integrar o seu grupo de investigação, não deixando de agradecer aos HoTI por me acolherem durante todo este tempo.

Tenho também que agradecer à minha família, pelo apoio incondicional não só ao longo deste percurso, mas em toda a minha vida. Gostaria principalmente de agradecer à minha mãe, que desde o primeiro dia foi o meu maior exemplo.

Como não poderia deixar de ser, tenho que também agradecer aos amigos que fizeram parte deste percurso. Agradeço à Bruna por estar ao meu lado ao longo de todos estes anos e por ser mais do que uma amiga – uma verdadeira irmã.

Também tenho de agradecer ao Noah. Obrigado pelos check-ups e pelo encorajamento. Agradeço também o entretenimento quase diário providenciado pelas tuas stories. Estou extremamente grato pela amizade de ambos.

Tenho também de expressar a minha sincera gratidão à Sara PP e à Sara não PP, que, embora partilhem quase o nome inteiro (e talvez uma homologia de 99%), são ambas especiais à sua maneira. Agradeço-vos por sempre me receberem de braços abertos e pelo apoio incondicional. Um especial obrigado ao Nuno, uma das pessoas mais singulares que já tive o privilégio de conhecer. A tua “childlike wonder”, curiosidade e vontade de aprender são verdadeiramente únicas. À Teresa, agradeço profundamente a tua amizade, enorme paciência, e os teus belos espetáculos de stand-up comedy. Aproveito este momento para reforçar o quão orgulhoso estou de todos vocês.

Um obrigado a Manu, por ser uma pessoa extremamente bondosa, carinhosa e genuína a si mesma. Obrigado por tornares os dias no bloco de cimento um pouco mais alegres.

Um obrigado também à Isa, dona de todas as palavras quando estas me escapam. Desde os rambles diários acerca de personagens fictícios a questões filosóficas, para mim há algo que se destaca. Obrigado por me ensinares “how to find a world in a rock”, a vida tornou-se muito mais bonita e “true blue”.

Um obrigado muito especial ao João por estar sempre disponível para me ajudar com tudo, mesmo quando não tinha qualquer responsabilidade. Ensinaste-me imenso ao longo deste ano, não só sobre ciência, mas sobre perseverança e força de vontade. Obrigado por seres o nosso pequeno raio de sol.

Por fim, há ainda uma pessoa que não posso deixar de mencionar. A minha mais sincera gratidão vai para a Lu, que ao longo deste ano foi o meu maior apoio. Obrigado por todos os dias e sem exceção, me arrancares um sorriso com uma facilidade incrível. És, sem dúvida, uma das pessoas mais bonitas que já tive o privilégio de conhecer.

Funding

This work was funded through National funds by Fundação para a Ciência e Tecnologia through the projects identified with the following DOI: EXPL/BIA-BQM/1170/2021 and 10.54499/2022.03635.PTDC.

Scientific Outreach

Part of the introduction of this thesis is published in a review article:

- Fonseca, Ó.; Ramos, A.S.; Gomes, L.T.S.; Gomes, M.S.; Moreira, A.C. New Perspectives on Circulating Ferritin: Its Role in Health and Disease. Molecules 2023, 28, 7707.

Part of the data presented in this dissertation was presented at the 6th Meeting of Medicinal Biotechnology at Escola Superior De Saúde Do Politécnico Do Porto (poster presentation).

- Ramos, A.S., Fonseca, O., Gomes, M.S., Silva, T., Moreira, A.C., Macrophages' metabolism impacts Hepatocyte viability – an in vitro study, 6th Meeting of Medicinal Biotechnology at Escola Superior De Saúde Do Politécnico Do Porto, May 17th, 2024

While developing my master's thesis, I enrolled in an Introductory Course in Laboratory Animal Science (October 2023 – February 2024) under the EU directive 2010/63/EU. Functions (A) and (D): Mice and Rats species-specific and got the respective certification from DGAV - Direção-Geral da Alimentação e Veterinária, July 2024.

Resumo

O ferro é um elemento essencial para os organismos devido ao conjunto de processos biológicos em que participa. No entanto, na sua forma livre, tem consequências nefastas para o organismo. Assim, o seu armazenamento, absorção e distribuição são rigorosamente controlados.

Durante uma infeção, os agentes patogénicos tentam aceder ao ferro do hospedeiro, uma vez que a disponibilidade de ferro está intimamente correlacionada com a proliferação bacteriana. O hospedeiro, no entanto, está munido de diversas estratégias antimicrobianas que restringem o acesso do patogénio ao ferro. Um exemplo disso é a redistribuição deste elemento. No entanto, esta alteração acarreta diversas consequências, nomeadamente a possibilidade de lesão de tecidos.

O fígado é um órgão multifuncional que orquestra inúmeros processos vitais para o organismo. Estes englobam processos de imunidade, metabolismo, síntese e destoxificação. Os hepatócitos são as células parenquimatosas predominantes neste órgão e desempenham um papel essencial no controlo dos níveis sistémicos de ferro, nomeadamente através da produção de hepcidina.

Compreender os mecanismos de redistribuição do ferro durante a infeção crónica é crucial para poder eficazmente realizar a sua modelação não só para controlar os agentes patogénicos, mas também minimizar os efeitos adversos para o hospedeiro. O nosso grupo já tinha demonstrado que a distribuição do ferro no hospedeiro sofre alterações durante a infeção crónica por micobactérias in vivo. Os macrófagos, componentes essenciais do sistema imunitário inato, produzem Ferritina-H, que é essencial para a distribuição do ferro no fígado.

Como tal, a hipótese por trás deste estudo é que durante a infeção, macrófagos hepáticos libertam componentes cujo efeito nos hepatócitos vizinhos é importante para a resposta imunitária relacionada com o ferro, destacando a importância das interações intercelulares.

Apesar de progressos na compreensão das funções dos hepatócitos, a comunicação com os macrófagos permanece pouco explorada. Este estudo aborda essa lacuna de conhecimento e procura investigar a comunicação hepatócito-macrófago, particularmente durante a infeção.

Com base nisto, estabelecemos um modelo in vitro de comunicação parácrina utilizando células AML 12, uma linha celular de hepatócitos de murganho e macrófagos derivados da medula óssea (BMMs).

Os nossos resultados sugerem que o meio condicionado de BMMs não só diminui a viabilidade da AML12 como também altera o transcriptoma e o proteoma relacionados com o metabolismo do ferro das AML12.

Palavras-chave: Hepatócitos, Macrófagos, Comunicação Intercelular, Homeostasia Hepática, Metabolismo do Ferro

Abstract

Iron is an essential element for living organisms due to the multiplicity of processes it engages in. However, in its free form, it has nefarious consequences for the organism. Thus, iron storage, absorption, and distribution are tightly regulated.

In their quest for survival during infection, pathogens try to access the host's iron since iron availability is closely correlated with bacterial proliferation. The host, however, is armed with several antimicrobial strategies that restrict the pathogen's access to iron. An example of this is iron redistribution. Nevertheless, this alteration leads to several consequences, namely potential tissue destruction.

The liver is a multifunctional organ and orchestrates vital processes encompassing immunity, metabolism, synthesis, and detoxification. Hepatocytes are the predominant parenchymal cells in this organ and play an essential role in governing systemic iron levels through hepcidin production.

Understanding the mechanisms of iron redistribution during chronic infection is crucial for effectively modulating them to enhance pathogen inhibition while minimising adverse effects for the host. Our group has previously shown that host iron distribution is altered during chronic mycobacterial infection in vivo. Macrophages, crucial innate immune system components, produce H-Ferritin, which is essential for liver iron distribution.

As such, the hypothesis behind this study is that during infection, liver macrophages release components whose effects on neighbouring hepatocytes are critical for the iron-related immune response, highlighting the importance of intercellular interactions.

Despite advances in understanding hepatocyte functions, communication with macrophages remains underexplored. This study intends to address this knowledge gap by investigating hepatocyte-macrophage communication, particularly during infection.

Building upon this, we established a paracrine communication in vitro model using AML 12 cells, a murine hepatocyte cell line, and Bone Marrow-derived Macrophages (BMMs). Our results suggest that BMM-conditioned medium decreases AML12 viability in a quantity-dependent manner and alters AML12's transcriptome and proteome related to iron metabolism.

Keywords: Hepatocytes, Macrophages, Intercellular Communication, Liver Homeostasis, Iron Metabolism

Table of Contents

List of Figures

List of Abbreviations

APPs	Acute-Phase Proteins
AML12	Alpha Mouse Liver 12
BMMs	Bone Marrow-Derived Macrophages
BSA	Bovine Serum Albumin
CFUs	Colony Forming Units
CT	Cycle Threshold
DTT	Dithiothreitol
DMT1	Divalent Metal Transporter-1
DMEM	Dulbecco's Modified Eagle Medium
Dcytb	Duodenal cytochrome b
EP	Erythroid Precursor
ELISA	Enzyme-Linked Immunosorbent Assay
EDTA	Ethylenediaminetetraacetic Acid
ECM	Extracellular Matrix
FAC	Ferric Ammonium Citrate
FT	Ferritin
FPN	Ferroportin
FBS	Foetal Bovine Serum
HBSS	Hank's Balanced Salt Solution
HSCs	Haematopoietic Stem Cells
Hmox-1	Haem oxygenase 1
HFE	Haemochromatosis Protein
Fth1	H-Ferritin gene (murine)
FTH	H-Ferritin protein
HRP	Horseradish Peroxidase
Hprt1	Hypoxanthine guanine phosphoribosyl transferase gene
IFN-γ	Interferon-γ

ITS	Insulin, Transferrin, Selenium
KCs	Kupffer Cells
LCCM	L929 Cell Conditioned Medium
Ftl	L-Ferritin gene
FTL	L-Ferritin protein
LEAP	Liver-Expressed Antimicrobial Peptide
LSECs	Liver Sinusoidal Endothelial Cells
M-CSF	Macrophage Colony-Stimulating Factor
MOI	Multiplicity Of Infection
NOS2	Nitric Oxide Synthase
NPCs	Non-Parenchymal Cells
NTM	Nontuberculous Mycobacteria
NF-κB	Nuclear Factor-kappa B
PVDF	Polyvinylidene Difluoride
PBS	Phosphate Buffered Saline
PI	Post-Infection
PIC	Protease Inhibitor Cocktail
ROS	Reactive Oxygen Species
qRT-PCR	Quantitative Reverse Transcription Polymerase Chain Reaction
RT	Room Temperature
SD	Standard Deviation
SRB	Sulforhodamine B
STAT3	Signal Transducer and Activator of Transcription 3
Tf	Transferrin
TfR	Transferrin Receptor
Tfsat	Transferrin saturation
TBST	Tris Buffered Saline with Tween 20
TNF-α	Tumour Necrosis Factor-α

I – Introduction

1. Iron

1.1. Iron, an Essential Element

Iron is one of the Earth's most prevalent elements, being indispensable for life. Iron's significance spans diverse biological realms despite only being a trace element. It serves as a vital component for the functionality of several living organisms. Inclusively, it has been recently shown that even *Lactobacillaceae*, which were once deemed independent of iron, depend on this mineral (1).

This transition metal from the d-block exhibits remarkable flexibility in transitioning between different oxidation states, predominantly encompassing Fe^{2+}, Fe^{3+}, and, to a lesser extent, Fe^{4+}. This iron oxidation form is typically found as an intermediate in specific enzymatic reactions (2, 3). These dynamic interconversions allow iron to selectively bind to different ligands, with oxygen, nitrogen, and sulphur atoms being the preferred ones. Due to its distinctive chemical attributes, iron is the favoured cofactor for multiple proteins. As a result, iron is integral to plenty of biological processes, including, but not limited to, cell proliferation, cell differentiation, mitochondrial respiration, nucleic acid synthesis, and oxygen transportation (4, 5).

The intricate interplay of iron within biological systems is exemplified by the spectrum of diseases derived from the disruption of iron metabolism. Insufficient iron levels often manifest as iron deficiency anaemia, predominantly affecting preschool children and women of reproductive age (6). Conversely, surplus iron may result in tissue iron overload disorders, such as haemochromatosis, leading to cytotoxic effects due to its redox activity. When in its unbound state, iron exacerbates the generation of Reactive Oxygen Species (ROS) and lipid peroxidation, leading to detrimental outcomes at a cellular level, such as the occurrence of ferroptosis (7).

Humans have evolved a sophisticated molecular system to regulate bodily iron levels. Iron exists predominantly in protein-bound forms in the mammalian body to mitigate its reactive nature and fulfil essential physiological roles. Free iron is rare due to its propensity to catalyse the formation of harmful free radicals; thus, the body employs transport proteins like Transferrin to safely transport iron through the bloodstream to various tissues. Once inside cells, excess iron is sequestered within Ferritin, the primary iron storage protein, safely storing iron inside the cells and releasing it when needed. In the immune response context, lactoferrin binds iron with high affinity, particularly in bodily

fluids like saliva. This makes it unavailable for microbial use, which helps limit bacterial growth and infection (8). The majority of functional iron, however, resides within the haem groups of haemoglobin in red blood cells. There, it plays a pivotal role in oxygen transport, ensuring cellular respiration across the body's tissues (9). Haemoglobin and haem are captured by haptoglobin and haemopexin, respectively. These bindings ensure the safe maintenance and transport of iron and haem between host cells. Additionally, the hormone hepcidin plays a crucial role in tightly regulating blood iron levels (10). These intricacies of iron metabolism regulation and the role of each protein will be addressed in detail in the following section.

1.2. Iron Metabolism

Several cells are involved in iron metabolism; enterocytes, macrophages, and hepatocytes deserve special attention. While enterocytes primarily absorb dietary iron, macrophages are responsible for iron recycling. These cells contribute to the release of iron into circulation, which is subsequently sequestered by hepatocytes, acting as the primary reservoir for iron storage (11). A finely tuned protein network is responsible for the interplay between iron influx, efflux, storage, and distribution, thus ensuring the maintenance of overall physiological homeostasis. This is of extreme importance as both deficient and excessive amounts of iron can disrupt normal physiological processes. An overview of these processes is illustrated in Figure 1.

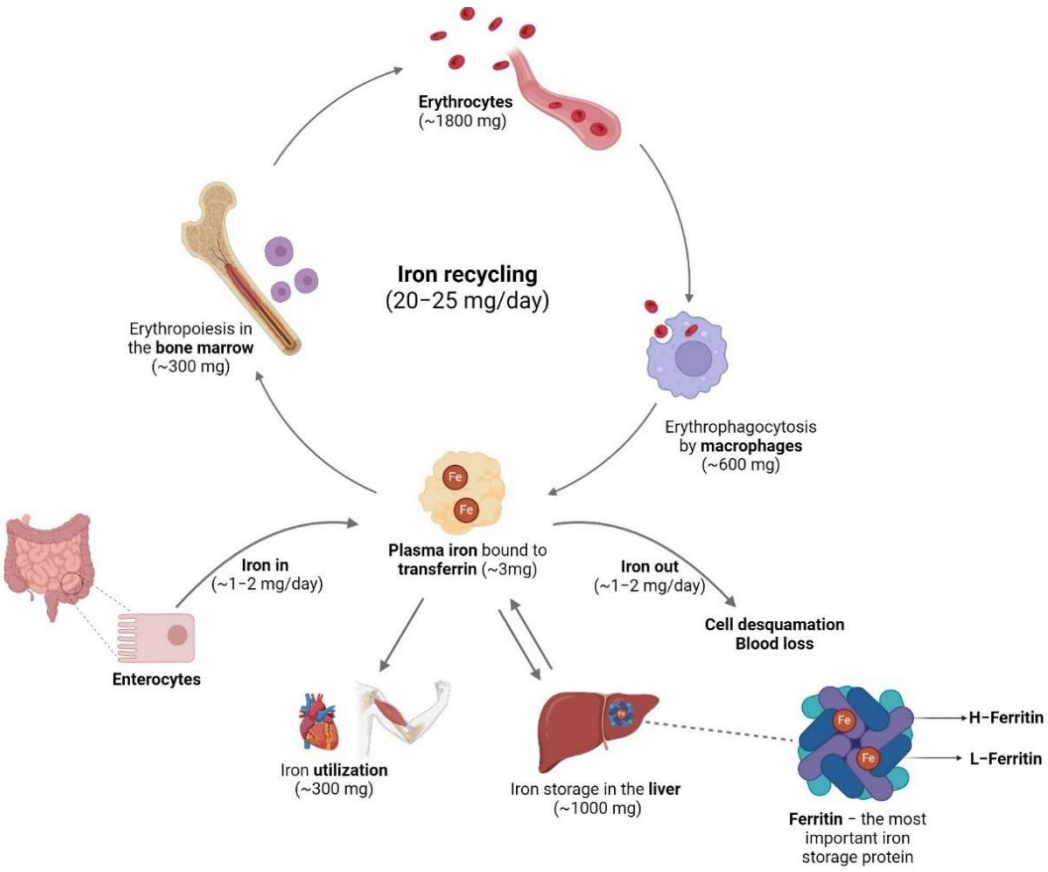

Figure 1. Overview of mammals' iron metabolism. Enterocytes absorb dietary iron. In general, the amount of iron ingested daily is roughly the same as the iron lost through cell desquamation and blood loss. Besides exogenous iron, the body also has mechanisms that allow for iron recycling, namely through macrophages. These cells can recover iron from the phagocytosis of old or senescent red blood cells. Iron circulates through the organism bound to Transferrin (Tf), allowing for the utilisation of this mineral in the body. Iron storage is essentially ensured by Ferritin (FT) inside this protein's nanocage. Image from Fonseca, Ramos *et al.*, (2023).

The body maintains steady iron levels by continuously recycling iron from red blood cells. In mammals, active iron excretion mechanisms are lacking, with minimal losses occurring through processes such as skin shedding, sloughing of intestinal epithelial cells, bleeding, and urinary excretion (12). To compensate for these minor losses, individuals typically obtain iron from their diet (~1–2 mg per day). As aforementioned, dietary iron absorption predominantly occurs in enterocytes, as depicted in Figure 2A (13).

Non-haem iron crosses the apical membrane of these cells via the Divalent Metal Transporter-1 (DMT1). However, this transporter exclusively internalises metals in their 2+ reduction state. Since dietary iron typically exists in its 3+ form (Fe^{3+}), it requires prior reduction by the Duodenal cytochrome b (Dcytb) ferrireductase (14). It is possible for iron in its haem form to also undergo absorption. However, despite documentation of non-haem iron internalisation, the mechanisms responsible for haem iron absorption have not been determined yet. Within enterocytes, haem undergoes the action of Haem oxygenase 1 (Hmox-1), leading to the release of free iron and other components such as carbon monoxide and bilirubin (12). Subsequently, free iron follows analogous processing as inorganic dietary iron (4).

Post-absorption, iron may undergo various pathways depending on bodily needs. Primarily, iron supports erythropoiesis within the bone marrow. Following damage or senescence, erythrocytes are phagocytosed by macrophages, facilitating the recovery of haem iron for recycling (Figure 2B). This ensures iron availability for synthesising new erythrocytes or other physiological processes (15). Hepatocytes (Figure 2C) manage iron storage, sequestering this mineral within Ferritin (FT) or releasing it into circulation via Transferrin (Tf), as required (11).

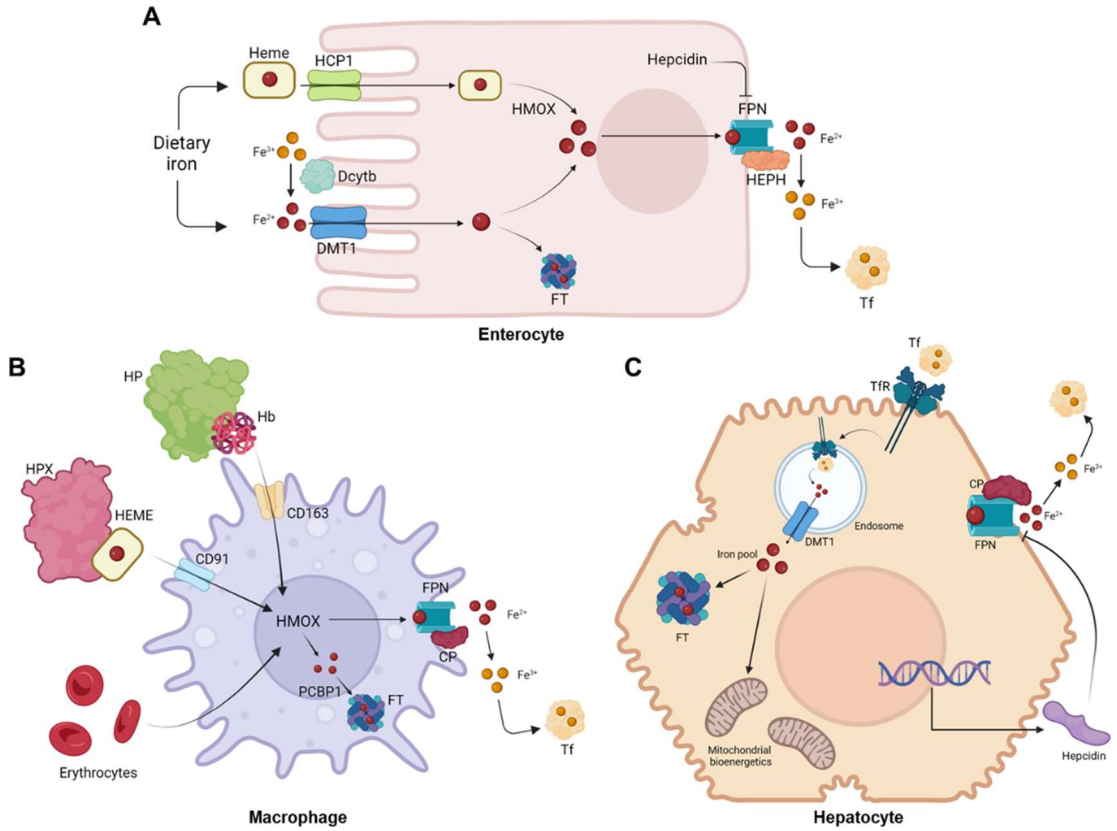

Figure 2. Illustrated iron metabolism molecular mechanisms. Abbreviations: CD163 – Cluster of Differentiation 163, haemoglobin-haptoglobin receptor; CD91 – Cluster of Differentiation 91, also known as Low-Density Lipoprotein Receptor-Related Protein 1 (LRP1) or α2-macroglobulin receptor; CP – Ceruloplasmin; Dcytb – Duodenal cytochrome B; DMT1 – Divalent Metal Transporter 1; FPN – Ferroportin; FT – Ferritin; Hb – Haemoglobin; HCP1 – Haem Carrier Protein 1 or Proton-Coupled Folate Transporter (PCFT); HEPH – Hephaestin; HMOX – Haem oxygenase; HP – Haptoglobin; HPX – Haemopexin; PCBP1 – Poly(RC) Binding Protein 1; Tf – Transferrin; TfR – Transferrin Receptor. Image from Fonseca, Ramos *et al.*, (2023).

The main protein responsible for intracellular iron storage is FT. This large, spherical protein stores iron within its hollow shell (16). Beyond its role as an iron repository, FT avoids the harmful effects of free iron and is also of major importance in immune modulation (16-18). While predominantly cytosolic, FT has also been detected in the nucleus (19, 20), mitochondria (21), and serum (22). Cytoplasmic FT comprises 24 protein subunits, which form the apoferritin shell, weighing approximately 450 kDa. This framework has the capacity to accommodate over 4000 Fe^{3+} atoms and is constituted of two subunits: H-Ferritin (FTH) and L-Ferritin (FTL), each weighing around 20 kDa (23). In humans, these subunits are encoded by separate gene loci (24). The relative abundance of FTH and FTL subunits within the apoferritin shell varies depending

on the tissue, with each subunit also exhibiting distinct functions (17). FTH contains a ferroxidase domain responsible for the conversion of ferrous (Fe^{2+}) to ferric iron (Fe^{3+}), the form that can be stored (25). Only FTH possesses the oxidising capability due to the absence of a ferroxidase centre in FTL. Nevertheless, FTL fulfils other roles, enhancing protein stability and iron-binding activity (26). Mechanisms for iron release from FT remain elusive, potentially involving FT degradation within lysosomes. Interestingly, the proportions of L and H subunits may vary depending on cell type, physiological status, and responses to infection or inflammation (3).

Ferroportin (FPN), the only known mammalian iron exporter, mediates iron release from cells under the regulation of hepcidin, also known as LEAP for Liver-Expressed Antimicrobial Peptide (27, 28). Hepcidin, a liver-derived peptide hormone, was initially identified as a peptide primarily synthesised by hepatocytes, with the ability to inhibit bacterial and fungal growth in vitro (27, 28). Despite its antimicrobial properties, the precise mechanism by which hepcidin exerts its bactericidal effects remains unclear. As such, its functional significance in vivo requires further elucidation. Subsequent research has unveiled hepcidin's pivotal role in iron homeostasis. By regulating blood iron levels, hepcidin plays a crucial role in restricting the proliferation of pathogenic microorganisms within the host (29). Rather than interacting directly with iron, hepcidin exerts its effects by binding to FPN. This binding by itself can lead to a decrease in FPN's activity, or it can promote internalisation and subsequent lysosomal degradation (30-33).

Although this protein is expressed in hepatocytes, they are not the only cells in which FPN is present, being also found in macrophages and enterocytes (34). Intestinal epithelial cells absorb iron from the intestinal lumen and transport it into the bloodstream via FPN, where it can bind to Tf for systemic distribution. Conversely, macrophages recycle haem iron from phagocytosed damaged or senescent red blood cells and release it into circulation through FPN. Hepcidin binds to FPN, promoting its internalisation and degradation. Elevated hepcidin levels reduce FPN availability, thereby decreasing iron absorption and recycling, ultimately reducing blood iron concentration. (10, 35, 36).

In conditions of iron overload, there is an elevation in hepcidin levels, triggering a reduction in FPN levels (37). Consequently, the export of iron diminishes, leading to an increase in intracellular iron accumulation and a decrease in circulating iron levels. Conversely, in conditions of anaemia or hypoxia, hepcidin levels decrease (38). This results in reduced degradation and heightened cell surface expression of FPN, facilitating a greater iron efflux to boost circulating iron levels. Iron released by FPN undergoes oxidation catalysed by ceruloplasmin, a ferroxidase, converting Fe^{2+} to Fe^{3+}

once more. The resultant Fe^{3+} subsequently binds to Tf (39). Therefore, iron mobilisation and erythropoiesis are stimulated (31).

Tf predominantly serves as the primary vehicle for iron distribution through the body. Transferrin saturation (Tfsat) levels, indicated as a percentage, are a pivotal biomarker for characterising iron metabolism disorders, with deviations from the norm indicating either deficient (<20%) or excessive (>50%) iron quantities (40, 41).

In humans, Tf is a single polypeptide chain weighing approximately 76 kDa, primarily synthesised in the liver. Its structure comprises two globular domains located at the N- and C-termini. Remarkably, each domain exhibits a high affinity for binding one iron ion, albeit reversibly. Consequently, a single Tf molecule can accommodate and transport two Fe^{3+} ions within the bloodstream (13).

Under normal physiological conditions, most of the iron in the bloodstream is bound to Tf. Cells require a Transferrin Receptor (TfR) to internalise iron from Tf. Transferrin-iron complexes exhibit a strong affinity for TfR, unlike Transferrin devoid of iron, and are subsequently internalised via endocytosis. Upon exposure to the acidic environment of the endosome, Tf releases its iron cargo. This iron is then reduced and transported to the cytosol through the action of DMT1, expressed in the endosome membrane. Meanwhile, the Tf molecule returns to the bloodstream (42). Although this pathway represents the primary mechanism by which cells acquire iron, TfR-independent iron uptake has also been documented (43-45).

1.3. Iron Metabolism During Infection

Beyond its pivotal role in cellular physiology, iron is a coveted nutrient for both macro- and microorganisms. This becomes particularly evident in infection settings where the dynamic interaction between host and pathogen unfolds. In such scenarios, a pursuit for iron ensues as the pathogen seeks to acquire this essential element from the host. By securing a supply of iron, the pathogen facilitates the establishment of infection and, concomitantly, ensures its own proliferation and survival (12). To thrive within a host, bacteria must acquire adequate iron levels. To do so, pathogens can employ specialised iron-chelating biomolecules known as siderophores to scavenge iron from their milieu (46). To counter this tactic, the host deploys defensive measures to restrict iron availability to inhibit bacterial proliferation (47). Circulating iron levels often decrease to limit pathogen access to this vital element (24) and also the production of siderophore-binding proteins such as lipocalin 2, thereby avoiding the pathogen's iron access (48).

Different bacterial species, however, have various strategies to manipulate host iron homeostasis (24). For example, Gram-positive bacteria like *Listeria* can alter host iron distribution by influencing FPN expression (49). During *Mycobacterium avium* infection, it has been observed that murine macrophages increase FTH expression while FTL levels remain stable, likely due to FTH's heightened responsiveness to microbial or inflammatory stimuli (50, 51).

Mycobacterium avium, part of the Nontuberculous Mycobacteria (NTM) group, colonises intestinal or respiratory mucosa, evading host defences by surviving within macrophages. Although most individuals do not develop disease, those who are immunocompromised or have underlying conditions are at increased risk, making *M. avium* an opportunistic pathogen (52).

Previous research from our group, using a murine model, demonstrated that FTH from a myeloid origin plays a role in iron redistribution during infection by storing iron within macrophages. (24, 53).

The downregulation of ferroportin in macrophages – directly by pathogens, immune mediators, or indirectly through hepcidin – leads to iron accumulation in these cells during infection. However, since *M. avium* resides within macrophages, this iron buildup is advantageous to the bacteria rather than the host.

Interestingly, our group showed that in mice with a conditional deletion of *Fth1* in myeloid cells (*Fth1*$^{-/-}$), macrophages showed reduced intracellular iron levels associated with increased ferroportin expression, causing iron to accumulate primarily in parenchymal cells (24). This redistribution reduces iron availability for *M. avium*, slowing bacterial growth and enhancing host defence.

Serum Ferritin, in basal conditions, was believed to be only formed of L subunits. However, total serum Ferritin levels in *M. avium*-infected mice were higher in WT mice compared to *Fth1*$^{-/-}$ mice. Moreover, the group showed that FTH has a myeloid origin (24). The elevated synthesis of FTH by macrophages during *M. avium* infection likely results in the release of H-chain-containing Ferritin into the bloodstream, suggesting that FTH plays a significant role in systemic and local iron redistribution (24).

2. The Liver

The liver, the largest solid organ in the human body, is responsible for over 500 critical functions encompassing immunologic, metabolic, synthetic, and detoxification processes. Its architecture is characterised by a repetitive, multicellular structure, with hepatocytes as the predominant parenchymal cells, accounting for 70-85% of the liver's total volume (29). In addition to hepatocytes, the liver is home to various supporting cells, including endothelial cells, Kupffer cells (the resident macrophage population), biliary ductal cells, and stellate cells (54). Thus, the liver plays a fundamental role in maintaining body homeostasis.

The hepatic lobule is the liver's fundamental structural and functional unit, characterised by its hexagonal architecture (Figure 3). Each lobule features a central vein, crucial in transporting intrahepatic metabolites. Encircling the lobule is the portal triad, composed of the hepatic portal vein, hepatic artery, and bile duct. The hepatic portal vein delivers nutrient-rich blood to the liver, whereas the hepatic artery provides oxygenated blood (55).

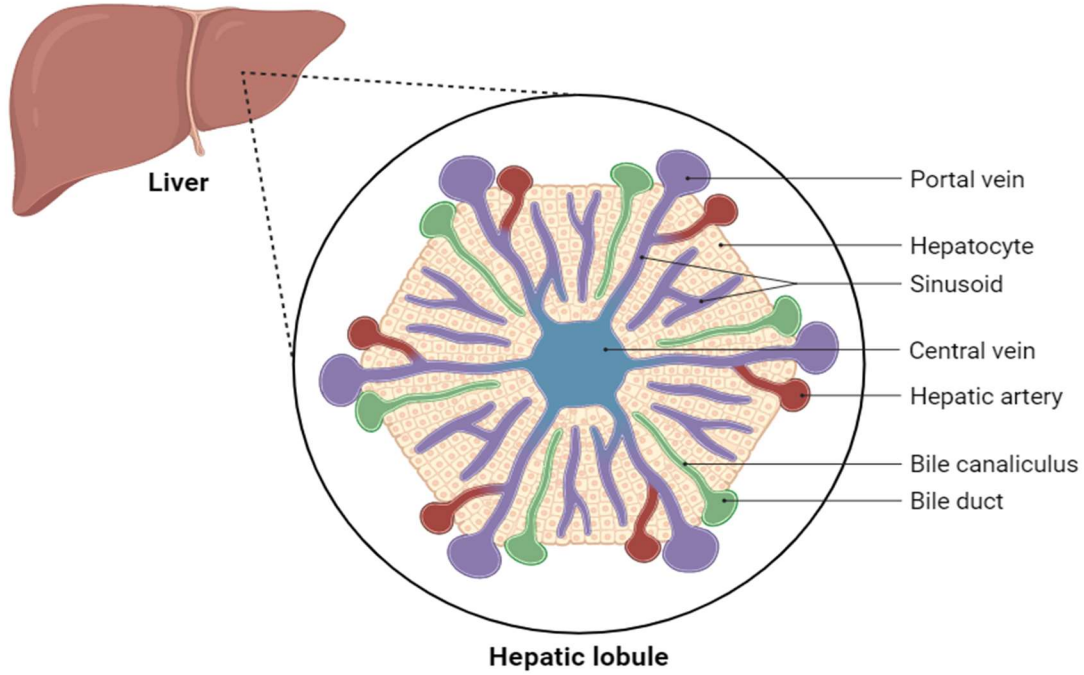

Figure 3. Schematic diagram of the liver lobule structure. Image created with BioRender.

2.1. Hepatocytes

Hepatocytes form plates that emanate from the central vein. These hepatocyte plates are interspersed with hepatic sinusoids, capillary-like channels formed by merging terminal branches from the hepatic portal vein and hepatic artery. Additionally, adjacent hepatocytes are linked by bile canaliculi, which facilitate bile collection and transport. Liver Sinusoidal Endothelial Cells (LSECs) construct the sinusoidal wall, enabling the exchange of materials between hepatocytes and sinusoidal blood within the Disse space, the region between hepatocytes and LSECs (56). Kupffer cells (KCs) reside in the lumen of hepatic sinusoids, extending along LSECs. In contrast, hepatic stellate cells are located within the Disse space, creating a separation between hepatocytes and LSECs alongside the Disse space components (56). The complex interactions among these liver cells maintain the structural and functional integrity of hepatic lobules (57).

Hepatocytes are continuously engaged in the production and secretion of various proteins essential for innate immunity, with many of these proteins experiencing elevated levels post-bacterial infection. Following pathogenic and inflammatory signals, hepatocytes rapidly produce and secrete innate immunity proteins into the bloodstream, known as Acute-Phase Proteins (APPs). Hundreds of APPs have been identified, each serving diverse functions, including the activation of innate immunity. These proteins either directly neutralise pathogens or orchestrate the immune system for efficient pathogen clearance, embodying an ancient immune defence mechanism that has evolved over time (29).

The production of APPs is regulated by a plethora of inflammatory cytokines such as IL-6, IL-22, IL-1β, Interferon-γ (IFN-γ), and Tumour Necrosis Factor-α (TNF-α), which activates Signal Transducer and Activator of Transcription Factor 3 (STAT3) and Nuclear Factor-κB (NF-κB). Pathogens promptly induce IL-6 expression in immune and epithelial cells, including hepatocytes (58-60).

In the domain of iron metabolism, hepatocytes stand as pivotal regulators, finely tuning systemic iron levels through the modulation of hepcidin, which can also be termed an APP, as previously discussed. Ferritin can also be considered an APP. This orchestration is facilitated by an array of hepatic proteins, such as Haemochromatosis Protein (HFE), among other key players. Additionally, it is noteworthy to emphasise the significant role of hepatocytes in the production of Tf, the primary iron transporter, which remains abundant within the liver's domain (61).

2.2. Macrophages

Macrophages play diverse and crucial bodily roles, extending far beyond from their well-known function in host defence against invading pathogens. These versatile cells are also vital for wound repair and maintaining tissue homeostasis. Notably, macrophages are key regulators of iron homeostasis. Erythropoiesis, the production of red blood cells, is the most iron-demanding process in vertebrates. Since erythrocytes have an average lifespan of only 120 days, macrophages recycle the iron from these cells to meet the body's ongoing iron demands. Every second, approximately 5 million erythrocytes, the average number per microliter of blood, are removed from circulation (62). Additionally, macrophages facilitate the formation of new red blood cells by supplying recycled iron and providing a supportive environment in the bone marrow, known as the erythroblastic islands (63).

Erythroblastic islands are specialised microenvironmental compartments where definitive mammalian erythroblasts proliferate and differentiate. The interactions within the erythroblastic island are crucial for the early and late stages of erythroid maturation (64). Early in erythroid maturation, macrophages provide nutrients and proliferative and survival signals to the erythroblasts, and later, they phagocytose the extruded erythroblast nuclei, completing the process of erythroid maturation (64).

Tissue-resident macrophages and macrophages derived from circulating monocytes, which derive from bone marrow precursor cells themselves, represent two distinct populations within the macrophage family. Tissue-resident macrophages are primarily established during embryonic development and persist in various tissues throughout adulthood. These macrophages possess unique characteristics tailored to their specific tissue environments, such as self-renewal capability and specialised functions (65). Examples include the liver's KCs and the spleen's red pulp macrophages. Conversely, Haematopoietic Stem Cells (HSCs) continually generate monocytes throughout life. The differentiation process involves multiple intermediate progenitor cells, ultimately leading to monocytes. These monocytes can either remain in the bone marrow, act as tissue-resident macrophages, enter the bloodstream to patrol vascular endothelium or contribute to tissue homeostasis elsewhere. Under pathological conditions, these circulating monocytes can differentiate into macrophages (66).

2.3. Macrophages in Iron Metabolism

As previously mentioned, macrophages play a crucial role in iron metabolism (Fig. 2B). After their maturation, Red Blood Cells (RBCs) have a lifespan of approximately 120 days in circulation. Afterwards, they are removed by macrophages in the spleen and liver (62). Kupffer cells and red pulp macrophages are vital in this process, as they phagocytose senescent and damaged erythrocytes (67). With the aid of Hmox-1, these macrophages extract iron from the haem groups within erythrocytes (Fig. 2B). This iron is then transported back to the bone marrow to be re-incorporated into forming erythrocytes and stored by FT. Additionally, macrophages can release FT via exocytosis to supply iron to Erythroid Precursors (EP). EPs internalise FT and release the iron intracellularly through acidification and proteolysis, making it available for haem synthesis (68).

Macrophages are also involved in manipulating iron metabolism to protect the host against pathogenic agents. This strategy, known as nutritional immunity, aims to deprive pathogens of iron (69). For extracellular pathogens, it is advantageous for the host to reduce extracellular iron levels, storing it inside the cells. This can be achieved by scavenging haem via iron scavengers like haptoglobin and haemopexin or by reducing FPN expression and inducing TfR and Hmox-1 (69, 70). The iron is subsequently stored inside FT. Furthermore, iron release from macrophages can induce Nitric Oxide Synthase (NOS2A), contributing to the microbicidal activity of macrophages (69).

2.4. Hepatocytes and Macrophages

Although the regulation of iron metabolism by macrophages and hepatocytes is well-described individually, less is known about how the communication between these cells occurs. Recent studies suggest that intercellular communication in the liver may involve extracellular vesicles (71) besides gap junctions (72) and mitochondria as a vehicle for molecule transportation (73). Research on hepatocyte-macrophage communication, particularly during infection, remains scarce. Macrophages are the most abundant immune cells in the liver, being crucial for microbial killing, tissue homeostasis, repair, inflammation, and development. They play a critical role in maintaining hepatic homeostasis and the underlying mechanisms of liver diseases (74). Despite the spatial organisation of hepatocytes within the liver being well characterised and described (75), there is still limited information on how macrophages are organised within their distinct

microenvironmental niches, both under basal conditions and during infection or inflammation.

As aforementioned, infection and inflammation significantly impact iron homeostasis through various mechanisms depending on the pathogen (24, 49, 76). Additionally, mice lacking HFE protein expression exhibit increased iron accumulation in hepatocytes, mimicking human HFE-related haemochromatosis. However, following systemic mycobacterial infection, there is a marked redistribution of liver iron, with iron accumulating in macrophages rather than hepatocytes (71).

The alterations in the liver's macrophage population directly influence hepatocytes regarding iron distribution during infection and the expression patterns of iron-related proteins, including ferroportin (24, 71).

3. In vitro Cell Models

Several in vitro models allow the study of hepatocytes and their interactions with non-parenchymal cells. Isolated primary human or rodent hepatocytes are ideal models for in vitro studies of hepatocyte biology. Despite advancements in cell culture conditions, primary hepatocytes face challenges such as limited ex vivo proliferation and eventual loss of hepatic phenotype (77). Because of this, many researchers use immortalised hepatocyte cell lines as a stand-in. The benefits, drawbacks, and application of various cell models are discussed in the sections that follow.

3.1. Primary Hepatocytes

Hepatocytes are typically bi-nucleated and form sheets within liver tissue. Despite their prolific growth in vivo, maintaining long-term cultures and proliferation of functional adult hepatocytes in vitro remains challenging. Primary hepatocytes tend to dedifferentiate into mesenchymal phenotypes after a few days in culture (78-80). Variations in sample types, isolation procedures, and other technical limitations complicate hepatocyte isolation and culture. These cells often require additional, sometimes costly, nutrients not included in classical media (81). Researchers worldwide have been optimising protocols to enable steady in vitro growth for downstream applications.

Initially, mechanical methods such as shaking with glass beads and filtering the liver through a cheesecloth were employed to isolate hepatocytes. Nonetheless, these methods had associated consequences since they caused extensive damage to the cell membranes and loss of hepatocyte function. These methods' low yield (5-10%) and

complexity led to the development of enzymatic perfusion techniques. Collagenase and hyaluronidase were perfused through the liver via the portal vein in rats (82). This enzymatic process enhanced the yield and integrity of the hepatocytes (83).

3.1.1. 2D Culture Models for Primary Hepatocytes

These cells are cultured on collagen-coated or gelatine-coated tissue culture wells or flasks post-isolation. This was done so as to replicate the hepatocyte micro-environment. The liver Extracellular Matrix (ECM) is mainly composed of type I and IV collagen and fibronectin. Collagen-coated plates extend hepatocyte culture longevity compared to uncoated plates (84, 85). Besides growing in pre-coated plates, hepatocytes can be covered by another layer of collagen hydrogel in a “sandwich configuration“. These cells maintain high levels of hepatic functions such as albumin secretion and cytochrome P-450 activities. Additionally, sandwich-cultured human hepatocytes can be sustained for more extended periods of time, being reported periods of longer than four weeks (86). The sandwich culture method more closely mimics in vivo tissue architecture, forming trabecular cell arrangements and abundant bile canaliculi networks (87).

3.1.2. 3D Cultures of Hepatocytes

As aforementioned, the biggest issue with conventional 2D systems is that primary hepatocytes undergo dedifferentiation and trans-differentiation into mesenchymal lineages. To address this, various improvements in hepatocyte culture have been explored, such as creating native-like niches incorporating growth factors, ECM components, and neighbouring cells. All these factors facilitate cell-cell and cell-ECM interactions.

Three-dimensional aggregates of hepatocyte spheroids or organoids are formed from self-organised cell clusters that do not attach to substrates. These aggregates can be generated using low-attachment plates, hanging drop cultures, microwells, matrigel cultures, rotating bioreactors, and polymeric scaffolds (88-90). While spheroids are made with liver cells, organoids are formed using resident hepatic stem cells or induced pluripotent stem cells co-cultured with non-parenchymal cells. The latter leads to the formation of self-organising 3D structures that more closely resemble natural liver structures when compared to spheroids (91-93). Despite resembling biological systems, spheroids and organoids remain technically challenging and demanding.

3.1.3. Co-Culture of Hepatocytes

The development of liver function is intricately linked to the environment-cell complex and cell-cell communication, encompassing direct physical contact and indirect paracrine signalling. Liver cell co-culture models can be categorised into direct co-culture and indirect co-culture based on their culture conditions. These co-culture systems can be applied to 2D and 3D hepatocyte cultures, cell lines, and primary hepatocytes.

Some studies highlight the importance of cell-matrix, cell-cell interactions, and soluble factors in maintaining liver cell functions in vitro, especially in primary hepatocytes. Therefore, direct co-culturing hepatocytes with Non-Parenchymal Cells (NPCs) enhances long-term hepatocyte maintenance. Random or micro-patterned co-cultures of hepatocytes with sinusoidal cells or diploid human fibroblasts have been shown to improve hepatic numbers and function (94).

Indirect co-culture involves culturing two or more types of cells, utilising a physical separation system (Figure 4). This system prevents direct cell-to-cell contact. This ensures communication is carried out through soluble cytokines or other signals, such as extracellular vesicles (95). Common materials for these separation systems include transwell cell culture plates and various natural or synthetic materials (57).

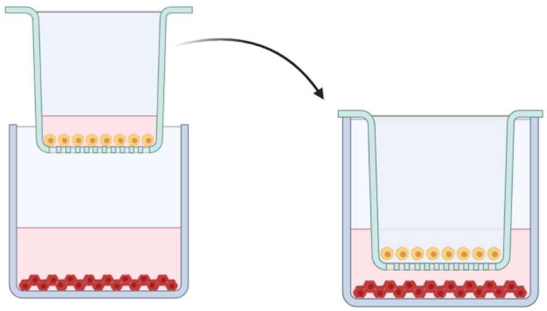

Figure 4. An example of an indirect 2D co-culture model of hepatocytes and macrophages. Hepatocytes are depicted as red cells in the bottom of the well, and macrophages, shown in yellow, are present in the transwells. Image created with BioRender.

3.1.4. Liver-on-Chip Models for Hepatocyte Cultures

Microfluidic and organ-on-chip systems are improved 3D models that address cellular requirements by introducing perfusion. This forced convection flow of medium enhances dissolved oxygen delivery to cells in culture (96).

To sum up, the usage of primary liver cells in research presents challenges due to their unpredictable availability, limited supply and self-renewal capacity, donor-

dependent variability, and sensitivity during isolation and culturing. As such, an alternative was needed.

3.2. Hepatic Cell Lines

Cell lines have fundamentally transformed scientific research. They are pivotal in vaccine development, drug metabolism and cytotoxicity testing, antibody production, gene function studies, artificial tissue generation, and the synthesis of biological compounds (97, 98). The widespread use of cell lines is evidenced by the extensive number of publications and the American Type Culture Collection (ATCC) Cell Biology Collection, which includes over 3,600 cell lines from more than 150 species.

Despite their utility, caution is necessary when substituting primary cells for cell lines. Cell lines should ideally replicate, to the greatest extent, the functional characteristics of primary cells. However, genetic manipulation of cell lines can alter their phenotype, native functions, and responsiveness to stimuli. Also, prolonged culturing can lead to genotypic and phenotypic variations due to serial passage and genetic drift, resulting in culture heterogeneity (99).

Another significant issue is contamination, either with other cell lines or mycoplasma. Walter Nelson-Rees highlighted the problem of cross-contamination, particularly with HeLa cells, in the early 1970s, revealing that many cell lines used globally and distributed by cell banks were contaminated with HeLa cells (100). This issue persists even after four decades. Rapidly proliferating contaminant cell lines can quickly overtake cultures, while mycoplasma contamination, which can go undetected for long periods, can drastically alter gene expression and cell behaviour (101). Thus, while cell lines are invaluable, it is crucial to use them with care and to verify key findings in primary cultures, when possible, to ensure accuracy.

Cell lines derived from hepatic tumours can be naturally immortal, but cells from healthy organs can also be artificially immortalised using various techniques, either biological, chemical or even physical. Immortalised cell lines are cost-effective, easy to handle, provide a limitless supply of biological material, and avoid ethical concerns associated with primary cell use (99). These cell lines are theoretically homogenous and genetically identical; their phenotypic stability ensures consistent and reproducible results (102).

Continuously growing hepatocytes are particularly valuable for research on hepatitis virus biology, hepatic drug uptake and xenobiotic metabolism, and

hepatotoxicity studies, particularly on enzyme capacities and investigations of general hepatocyte function (103-105).

Immortalised hepatocyte cell lines such as HepG2 and Huh7 are derived from hepatocellular carcinoma. These cell lines exhibit liver-like functions, including albumin synthesis (106) and the secretion of VLDL and triglycerides (107). However, their phenotype is more akin to liver cancer than to healthy liver tissue. Indeed, a study found that among 25 hepatocellular carcinoma cell lines, HepG2 and Huh7 had gene expression profiles most closely resembling primary hepatocellular carcinoma tumours (108). This finding underscores their suitability for studying hepatocellular carcinoma biology rather than normal hepatocyte biology.

Hepatocyte cell lines originating from healthy liver tissue may more closely resemble primary cells. Cell immortality is achieved when a cell loses its cell cycle checkpoint pathways. Various methods can induce immortality in cell lines. These include the ectopic expression of telomerase or Telomerase Reverse Transcriptase (TERT), mutations in p53 and *pRb* genes, or introducing oncogenes. Viral vectors facilitate these approaches by introducing TERT and oncogenes or mutating p53/pRb. Telomere elongation stabilises chromosomes, thereby rendering cells immortal (109). Oncogenes or viral vectors encoding oncoproteins can also transform cells into their immortal state by disrupting cell cycle checkpoints and regulators. Human Papillomavirus (HPV) and SV40 are commonly used vectors for such transformations (109).

Non-cancerous hepatocyte cell lines also exist and can be used as alternatives to primary cells in in vitro hepatocyte research. The AML12 cell line, derived from hepatocytes of transgenic mice overexpressing human Transforming Growth Factor α (TGF α) (110), is a non-tumorigenic cell line which has been used for investigating lipid metabolism, including conditions such as steatosis and non-alcoholic fatty liver disease (111, 112), as well as liver injury (113).

TGFα is a polypeptide that plays a critical role in regulating the growth of epithelial tissues. TGFα is present in the liver during embryonic development and shows a temporary increase during liver regeneration after partial hepatectomy. Its overproduction in cells with Epidermal Growth Factor Receptors (EGFRs) is often associated with malignant transformation. Proliferating hepatocytes produce and respond to TGFα through an autocrine mechanism (110). With this growth factor overexpression, these cells exhibit enhanced proliferating capacity and immortality.

Electron microscopy of these cells also displays typical hepatocyte features, including peroxisomes and structures resembling bile canaliculi. They also retain the capability of expressing high mRNA levels for multiple proteins including, but not limited to, albumin, alpha 1 antitrypsin and Tf (114).

Due to the technical and biological difficulties associated with the harvesting and maintenance of primary hepatocytes, in this study, we used the AML12 cell line as our hepatocytic model. Additionally, for the macrophage model we used primary macrophages, the Bone Marrow derived Macrophages (BMMs). This cell model has been established as a macrophage model in our group for a long time (53, 115, 116). BMMs are generated through the in vitro differentiation of haematopoietic precursors in the presence of Macrophage Colony-Stimulating Factor (M-CSF or CSF1) over a period of 7 days. This method produces a uniform population per mouse that exhibits several macrophage-like properties, although they do not perfectly mimic any specific in vivo resident or inflammatory macrophage population. Despite this, BMMs have been extensively utilised in macrophage research (117). Their versatility in being polarised and activated in various ways has established them as a standard reference for defining macrophage activation and polarisation nomenclature (118).

4. Objective

The hypothesis behind this study is that liver macrophages release molecules or cell components whose effects on neighbouring hepatocytes are critical for the iron-related inflammatory response during *M. avium* infection, highlighting the importance of intercellular interactions.

Despite advances in understanding hepatocyte functions, communication with macrophages remains underexplored. Elucidating the mechanisms of iron redistribution during chronic infection is vital to modulating them for more efficient pathogen inhibition without the attendant adverse effects on the host.

This study addresses this knowledge gap by attempting to investigate hepatocyte-macrophage communication. As such, the main objective of the project in which this thesis is inserted is to elucidate the molecular mechanisms of iron-related communication between macrophages and hepatocytes during mycobacterial infection using an in vitro model.

Building upon the host lab's previous research, we explored the mechanisms driving the iron circuit between macrophages and hepatocytes, using in vitro *M. avium* infection as a stimulus to study these interactions.

As such, this work's experimental model consisted of treating AML12 cells using BMM-conditioned medium. The first step was to assess how this treatment would affect AML12's viability. The next step was to investigate how this stimulus would affect these cells' basal transcriptome and proteome, particularly related to iron metabolism.

II – Materials and Methods

1. Chemicals

Unless stated otherwise, all chemicals and reagents were acquired from Sigma-Aldrich (St. Louis, MO, United States) and cell culture reagents from Gibco (Paisley, United Kingdom).

2. Bacteria

The strain of mycobacteria used in this work was *Mycobacterium avium* 25291, obtained from the American Type Culture Collection (Manassas, VA, United States). Aliquots were kept at -80ºC at a $2x10^9$ CFUs/mL concentration. Every time an inoculum needed to be prepared, a new aliquot was quickly thawed and homogenised using a vortex before the necessary volume was pipetted.

3. Mice

Mus musculus C57BL6 or BALB/c male mice were used in this work to collect bone marrow progenitor cells. This process will be further described in the sections below; 8-week-old animals were used. Importantly, all procedures carried out were performed by people certified by FELASA (Federation for Laboratory Animal Science Associations) under the approval of DGAV (Direção-Geral de Alimentação e Veterinária), the Portuguese national authority for animal health. Both supervisors of this thesis have a FELASA C certification, and I got the FELASA B certification during this internship.

4. Bone Marrow-Derived Macrophages (BMMs)

BMMs were derived from the bone marrow of both the femur and tibia of Non-Infected mice. Mice were euthanised, resorting to CO_2, and cervical dislocation was carried out as proof of death. The posterior legs were subsequently removed and separated from the hip using dissection scissors. The bones were then cleaned and separated. Following this, the extremities of each bone were cut to allow the insertion of a 26G needle attached to a syringe containing cold Hank's Balanced Salt Solution (HBSS). The bone marrow was then flushed into a 50 mL tube, 10 mL of HBSS were used to flush each bone. The resulting suspension was centrifuged for 10 minutes at 259 *g* at 4ºC. The obtained pellet, in which the cells were contained, was resuspended in Dulbecco's Modified Eagle Medium (DMEM) supplemented with 100 mM sodium

pyruvate,1 M HEPES, 200 mM L-glutamine and Foetal Bovine Serum (FBS). After that, the cell suspension was transferred to a tissue culture-treated plate containing DMEM + 10% of L929 Cell Conditioned Medium (LCCM) as a Macrophage Colony Stimulating Factor (M-CSF) source. The LCCM had already been prepared and frozen; each time it was necessary to use this supplement, a new aliquot was thawed and filtered using a 0.22 µm filter. Cells were then incubated overnight at 37ºC, 7% CO_2. The following day, the non-adherent cells, an indication of non-differentiated cells, were collected, and the plate was washed three times with cold HBSS to further collect cells that could have suffered deposition. Afterwards, this suspension was centrifuged for 10 minutes at 259 *g* at 4ºC and resuspended in complete DMEM. Cells were plated at a $4x10^5$ cells/mL density using DMEM/10% LCCM in 6-well plates (3 mL of suspension per well) or 24-well plates (1 mL of suspension per well). This procedure counts as day 0 of the differentiation process. On the 4th day of culture, 10% of each well-volume of LCCM was added to further differentiate the bone marrow progenitor cells into macrophages. On the 7th day of culture, the medium was renewed utilising warm DMEM/10% LCCM; the volume used for each well was the same as mentioned before.

4.1. BMM Infection and Bacterial Growth Assessment

When the macrophages were differentiated, on the 10th day of culture (115), these cells were infected with an *M. avium* 25291 suspension in DMEM (without LCCM). The multiplicity of infection (MOI) utilised was 1.5, which means that there is an expected average of 3 bacteria per 2 macrophages. The concentration of the prepared bacterial suspension was $5x10^6$ CFU/mL. This suspension was afterwards distributed in 6-well plates (600 µL per well) or 24-well plates (200 µL per well).

Following this, the cells were incubated for 4 hours at 37°C in 7% CO_2. After this period, they were washed four times with warm HBSS to remove non-internalised bacteria and then reincubated in the appropriate volume of warm DMEM/10%LCCM.

Additionally, the number of internalised bacteria (T_0) was determined by the colony-forming units (CFUs) method. This was done by using at least three wells of a 24-well plate. To do so, 10 µL of a 10% saponin solution was added to each designated well, which was scraped to release all intracellular bacteria. The lysates were posteriorly transferred to an empty glass tube. Serial 1:10 dilutions in H_2O+Tween 80 were then performed. Henceforward, the 3rd and 4th dilutions were plated into Middlebrook 7H10 medium (Becton, Dickinson and Company, Franklin Lakes, New Jersey, United States) supplemented with 10% of OADC supplement (Oleic acid, bovine Albumin, Dextrose, and Catalase).

Bacterial quantification was also performed 48h, 72h and 96h Post-Infection (PI) by the same method. The only difference was that the plated dilutions were the 3rd, 4th and 5th. In similitude, 7H10 plates were incubated for at least ten days at 37ºC before colonies could be counted and CFUs calculated.

4.2. Collection of BMM Lysates and Supernatants

Cell supernatants were collected at several time points (48h, 72h and 96h PI) from 6-well plates and stored at -80ºC. After the supernatant collection, cells were harvested to collect either protein lysates, RNA lysates, or cell lysates for iron quantification. Each of these processes will be detailed below.

Cell lysates for protein analysis were collected using a cold 5 mM Ethylenediaminetetraacetic Acid (EDTA)/Phosphate Buffered Saline (PBS) solution, followed by scraping to ensure all the cells were collected. The obtained cell suspension was centrifuged for 10 minutes at 2879 *g*. Then the pellet was resuspended in 100 µL of lysis buffer, which consisted of 1:1 RIPA buffer (150 mM NaCl, 1.0% NP-40, 0.5% sodium deoxycholate, 0.1% SDS, 50 mM Tris, pH 8.0, supplemented with Dithiothreitol (DTT) and Phenylmethylsulphonyl Fluoride (PMSF)) and PIC (Protease Inhibitor Cocktail) (Roche, Basel, Switzerland) mixture. All the procedures were performed at 4ºC. This protein extract was then stored at -80ºC.

Collecting cells for iron analysis was similar to the method described above. The only difference is that the 5mM EDTA/PBS solution used did not contain NaCl, but KCl instead, since sodium interferes with the iron quantification process. After centrifuging the cells, the supernatant was removed, and the pellet was not resuspended, being placed for 48 hours in an incubator at 37ºC to further dry any possible remaining supernatant.

RNA was also extracted from BMMs. To do so, the PureLink® RNA Mini Kit was used according to the manufacturer's instructions (AmbionTM, Invitrogen, Carlsbad, CA, United States). The samples were stored at -80 ºC before conversion to cDNA and qPCR analysis.

5. Quantitative Reverse Transcription Polymerase Chain Reaction (qRT-PCR)

The RNA was converted into cDNA utilising the First-Strand cDNA Synthesis Kit (NZYtech, Lisbon, Portugal) following the manufacturer's instructions. The samples were then placed in a Thermocycler (Bio-Rad Laboratories, Hercules, California, United States) using the following procedure: 25ºC for 10 minutes, 55ºC for 30 minutes and 85ºC for 5 minutes. The samples were then chilled at 4ºC before adding 1 µL of RNase. Afterwards, the samples were again placed in the Thermocycler and subjected to 37ºC for 20 minutes.

The cDNA was stored at -20ºC before use. To prepare the samples for the qPCR, the reaction mix was first prepared as follows: 350 µL of the probe (iTaq Universal SYBR Green – Bio-Rad Laboratories, Hercules, California, United States) and 35 µL of a specific pair of primers (forward and reverse) for each gene were added with 245 µL of water. Next, 19 µL of this mix was added to each well of a 96-well plate, which had previously been pipetted with 1 µL of cDNA. The qPCR was run on IQ5 (Bio-Rad Laboratories, Hercules, California, United States), where the cDNA was heated for 5 minutes at 94 ºC and entered a cycle that repeated itself 24 times, which was as follows: heating 30 seconds at 94 ºC, 1 minute at 30 ºC and 30 seconds at 72 ºC. At the end of the cycles, the samples were heated for 5 minutes at 72 ºC and kept at 4 ºC. Cycle Thresholds (CT) were obtained by the Bio-Rad Laboratories iQTM5 software and normalised to the housekeeping gene, Hypoxanthine-guanine phosphoribosyl transferase (Hprt1), (ΔCT), as shown in equation 1. A CT value, also known as Cycle Threshold, represents the cycle number at which a sample's reaction crosses a fluorescence threshold, indicating the detection of the target nucleic acid. Lower CT values indicate higher target sequence amounts, while higher CT values suggest lower amounts or possible issues in the process.

The next step was calculating the difference between the ΔCT values for the experimental and the control conditions, resulting in the ΔΔCT value (equation 2). Since all calculations are in logarithm base 2, equation 3 was applied to get the expression fold change.

$$\Delta CT = CT_{GI} - CT_{HG} \quad (1)$$

$$\Delta\Delta CT = \Delta CT_{E} - \Delta CT_{C} \quad (2)$$

$$\text{Fold change} = 2^{-\Delta\Delta CT} \quad (3)$$

GI – Gene of Interest; HG – Housekeeping Gene; E – Experimental Group; C – Control Group

Table 1. Primers list.

Gene	Sequence
Hprt forward	5'-GGTGGAGATGATCTCTCAAC-3'
Hprt reverse	5'-TCATTATAGTCAAGGGCATATCC-3'
Fth1 forward	5'-GCTGAATGCAATGGAGTGTGCA-3'
Fth1 reverse	5'-GGCACCCATCTTGCGTAAGTTG-3'
Ftl forward	5'-ACCTACCTCTCTCTGGGCTT-3'
Ftl reverse	5'-TGGCTTCTGCACATCCTGGA-3'
Tf forward	5'-ACCTGGAACAACCTGAAAGG-3'
Tf reverse	5'-GGCCAATACACAGGTCACAG-3'
Hamp1 forward	5'-CCTATCTCCATCAACAGATG-3'
Hamp1 reverse	5'-AACAGATACCACACTGGGAA-3'
Tfr forward	5'-GCAGCATTGGTCAAAACATGC-3'
Tfr reverse	5'-GCTTTGGGCATTTGCAACCC-3'

6. Hepatocyte Cell Line – AML 12 Cells

The hepatocyte cell line used in this work – AML12 cells – was purchased from the American Type Culture Collection (Manassas, VA, United States). AML12 (alpha mouse liver 12) cells were established from hepatocytes isolated from the normal liver of a 3-month-old mouse. This mouse (CD1 strain, line MT42) was transgenic for human TGF alpha. Upon receiving this cell line, it was frozen, resorting to liquid nitrogen to achieve a temperature of -130ºC, and kept in this condition until further use.

6.1. Handling Procedure

The vial in which the cells were stored at -130ºC was thawed rapidly with gentle agitation in a 37ºC water bath. The contents inside the vial were transferred to a centrifuge tube containing 9.0 mL of complete culture medium (DMEM F-12 supplemented with the following: 10% FBS, 10 µg/ml insulin, 5.5 µg/ml Transferrin, 5 ng/ml selenium, 40 ng/ml dexamethasone). The supplementation was carried out using a pre-made supplement designated as ITS (Insulin, Transferrin, Selenium) that already contained an adequate amount of the components listed. The dexamethasone solution was prepared by dissolving 1 mg of dexamethasone in 1 mL of ethanol; posteriorly, it was added to 49 mL of DMEM F-12. The tube was then centrifuged for 5 minutes at 300 *g* at Room Temperature (RT). The obtained pellet was then resuspended in 4 mL of complete medium and was dispersed in a 25 cm^2 flask (Corning Incorporated, Corning,

New York, United States) previously incubated with 5 mL of complete medium for at least 15 minutes to allow the medium to reach its appropriate pH (7.0 to 7.6). The culture was then incubated at 37ºC with 5% CO_2. The cell media were changed the day after the cells had been defrosted, utilising 10 mL of complete DMEM F-12 as described above. Following this, the media were renewed whenever necessary (2 to 3 times a week).

6.2. Subculturing Procedure

Once the cells had reached the desired confluence, they were split into different flasks. Firstly, the cell media were removed and discarded, and the cells were briefly rinsed with 2 mL of PBS 1x to remove all traces of FBS, which contains trypsin inhibitor. Following this, 2 mL of TrypLE 1x (ThermoFisher, Massachusetts, United States) was added, and the cells were observed under a Nikon eclipse Ts2 inverted microscope (Minato City, Tokyo, Japan) to oversee the detachment process. To make this process faster and gentler for the cells, they were placed in the incubator at 37ºC for approximately 10 minutes. The cell suspension was then collected and placed in a tube containing 4 mL of complete medium. This suspension was centrifuged at 300 *g* for 5 minutes. The supernatant was discarded, and the pellet was resuspended in 4 mL of complete media. This suspension was distributed into 3 different 25 cm^2 flasks containing 9 mL of complete medium. These flasks had already been incubated for at least 15 minutes before their usage to ensure that the proper pH of the media had already been established. After the second passage, the cells were transferred to 75 cm^2 flasks (Corning Incorporated, Corning, New York, United States) in a 1:3 or 1:4 dilution.

6.3. Cell Seeding

Similarly to what was described above, when the cells had the desired confluence, they could be seeded in plates to conduct experiments. The same procedure described in the Subculturing Procedure section was performed until the pellet resuspension. Here, the cells in the obtained suspension were counted, and the concentration was adjusted to $2.5x10^5$ cells/mL. These cells require plates to be coated for them to adhere. Two different kinds of plate coatings were tested, those being a 0.2% Gelatine (Gelatin from porcine skin) in PBS solution, or a 50 ug/mL collagen solution obtained from PureCol®, a 3 mg/ml Type I bovine atelocollagen solution (BICO, Gothenburg, Sweden) depending on the assay being conducted. Following this, the media were renewed whenever necessary (2 to 3 times a week).

6.4. Cryopreservation

The AML12 cells were cryopreserved at low passage numbers. To do so, the same procedure described in the Subculturing section was carried out, except after the centrifugation, the cells were resuspended in freezing media. This media is composed of complete media with 5% v/v DMSO. The obtained suspension was placed in cryotubes (ThermoFisher, Massachusetts, United States), which were then placed inside the Mr. Frosty™ freezing container (ThermoFisher, Massachusetts, United States), which was then placed at -80ºC overnight and transferred into liquid nitrogen afterwards. Once again, an analogous procedure to the Handling Procedure was carried out to defrost the cells when necessary.

6.5. AML12 Collection

The procedure for protein extraction, RNA extraction, and collection of lysates for iron analysis was analogous to what was performed for BMMs, detailed in the sections above.

7. Quantification of Cell Mass and Cell Viability

7.1. Cell Mass Determination by the Sulforhodamine B Colourimetric Assay

AML 12 cells were seeded in a 48-well plate using two cell densities ($1x10^5$ and $2.5x10^5$ cells/mL) (119). At each time point (24 to 144 hours), the culture medium was removed from the wells corresponding to that time point, and these were washed with PBS 1x. Posteriorly, the plate was returned to the incubator. This process was repeated every 24 hours until the end of the experiment. At the 72h time point, besides aspirating the culture medium and rinsing the wells with PBS, the cell medium from the remaining wells was changed.

After all the points had already been performed, 500 µL of 1% acetic acid in methanol was added to each well of the entire plate. The plate was covered with aluminium foil and placed at -20ºC overnight to promote cell fixation. The 1% acetic acid solution was discarded the following day, and the plate was placed, with the lid open, in a 37ºC incubator for approximately 1 hour. After this period, 250 µL of a 0.05% SRB solution was added to each well for another hour at the same temperature. After this solution had been discarded, the wells were thoroughly washed with a 1% acetic acid solution, and the plate was once again placed in the incubator to dry overnight.

Finally, 250 µL of 10 mM Tris-NaOH, pH 10, was added to each well, and the plate was placed in an orbital plate shaker at RT for 30 minutes. Then, 100 µL of each well was transferred to a 96-well plate. The absorbance was then read at 510 nm, and the background measurement was done at 620 nm in a Synergy™ Mx Multi-Mode Microplate Reader using the software Gen5 (BioTek, Winooski, VT, United States).

This essay was also conducted on 24-well plates by appropriately scaling up the necessary reagents.

7.2. Cell Viability Determination by the Resazurin Assay

Resazurin assays were performed in AML12 cells and BMMs using a similar methodology. To perform this assay, a 1.25 mM resazurin solution was freshly prepared in PBS 1x each time the assay was conducted. The solution was filtered using a 0.22 µm filter before adding it to the cells. Afterwards, 10% of the well volume of the resazurin solution was added to each well, and the cells were incubated at 37ºC. AML12 cells were incubated for approximately 2 hours, and BMMs were incubated for 5 to 6 hours. The fluorescence of resorufin, resulting from the reduction of resazurin by metabolic active cells, was measured at λ_{ex}=530 nm λ_{em}=590 nm in a Synergy™ Mx Multi-Mode Microplate Reader using the software Gen5 (BioTek, Winooski, VT, United States).

8. Detection and Quantification of Specific Proteins by Western blot

Before starting the western blot procedure, the protein content of the samples that would be analysed was quantified. To do so, the DC Protein Assay (Bio-Rad Laboratories, Hercules, California, United States) was used according to the manufacturer's instructions. Briefly, six serial dilutions of Bovine Serum Albumin (BSA) from 2 to 0.125 mg/mL were prepared as the standards for the assay. Following this, the working reagent (A') was prepared by adding 20 µL of reagent S to 1 mL of reagent A. Afterwards, 5 µL of each standard and each sample (Dilutions: AML12 1:10, BMM 1:3) was pipetted into a clean and dry microtiter plate followed by the addition of 25 µL of reagent A'. Finally, 200 µL of reagent B was added to each well and mixed for 5 seconds, pipetting up and down carefully. After 15 minutes, the absorbance of the plate was read at 750 nm. The samples were diluted in Laemmli SDS sample buffer (375 mM Tris pH 7.6, 9% (m/v) SDS, 50% (v/v) glycerol, 9% 2-mercaptoethanol (v/v), 0.075% bromophenol blue (m/v) in water) to a concentration of 5 µg/mL, denaturated at 95ºC for 5 minutes and loaded into a 10% SDS-polyacrylamide gel. Electrophoresis was

performed at 80 V for protein stacking, followed by 125 V for protein separation. Proteins were then electrophoretically transferred onto a Polyvinylidene Difluoride (PVDF) membrane for 90 minutes at 100 V.

After the membrane was blocked with 5% BSA in Tris Buffered Saline with Tween 20 (TBST) (50 mM Tris-HCl [pH 8], 154 mM NaCl, 0.1% Tween 20) for 2 hours at RT, membranes were incubated overnight at 4ºC with the primary antibodies according to the manufacturers' recommendations (Table 2). Membranes were washed three times for 5 minutes with TBST and incubated with the secondary antibody conjugated with Horseradish Peroxidase (HRP) (The Binding Site, Birmingham, United Kingdom in a 1:5000 dilution) in 1% BSA/TBST for one hour at RT. After this time, the membranes were rewashed thrice for 5 minutes with TBST. The membrane imaging was carried out using an HRP substrate (Luminata™ Millipore, Billerica, Massachusetts, United States) to release chemiluminescence. The intensity of the bands was measured using ChemiDoc (Bio-Rad, Hercules, CA, United States). The images acquired were analysed with ImageLab software (Bio-Rad Laboratories, Hercules, California, United States).

Table 2. Antibodies list.

Antibodies	Source	Identifier	Dilution
anti-FTH1	Cell Signalling Technology	4393S	1:1000
anti-FTL	Abcam	ab69090	1:1000
anti-Tf	Abcam	ab82411	1:1000
anti-TfR	Abcam	ab84036	1:1000

9. Quantification of TNF-α by Enzyme-Linked Immunosorbent Assay (ELISA)

TNF-α was quantified in BMM conditioned medium using the Legend Max™ ELISA kit (BioLegend, Inc., San Diego, California, United States). The first step in this protocol was to prepare all the necessary reagents according to the kit's instructions. Since the samples that were going to be analysed were solely cell supernatants, there wasn't a need for them to be previously diluted. The only preparation for these samples was a 10-minute centrifugation at 4ºC at 12 000 *g*. The remaining steps of the protocol were carried out as described in the manufacturer's instructions. The absorbance at 450 and 570 nm (for the background) was then read in a Synergy™ Mx Multi-Mode Microplate Reader using the software Gen5 (BioTek, Winooski, VT, United States).

10. Iron Quantification

Iron quantification was performed through atomic absorption spectrometry as previously described (53) by Professor Agostinho Almeida at Faculdade de Farmácia da Universidade do Porto.

11. Statistical Analysis

Data analysis was performed using the GraphPad Prism 8.0.1 program (GraphPad Software, Inc., La Jolla, CA, United States). Data are expressed as Mean ± Standard Deviation. The number of samples and replicates is indicated in the legend of each figure. Multiple comparisons between controls and each experimental time point were performed using an ordinary one-way ANOVA, with which the p-value was determined. Differences between groups were considered significant when the $p<0.05$.

III – Results

1. AML12 Characterisation

The cell model chosen to represent murine hepatocytes during this project was the Alpha Mouse Liver 12 cell line (AML12). This cell line was new in the laboratory, so characterising it was needed before performing any essays.

Fluorescence microscopy was conducted to assess these cells' possible fluorescent characteristics that could hinder follow-up assays. We verified that these cells did not exhibit any autofluorescence. We also evaluated cells' morphology in basal conditions using optical microscopy. These cells exhibit hepatocyte-like morphology, being regular, flat, polygonal cells with a granular cytoplasm (Figure 5). During the different experiments presented in this thesis, cells were always analysed under the microscope and showed similar morphology as those in this figure.

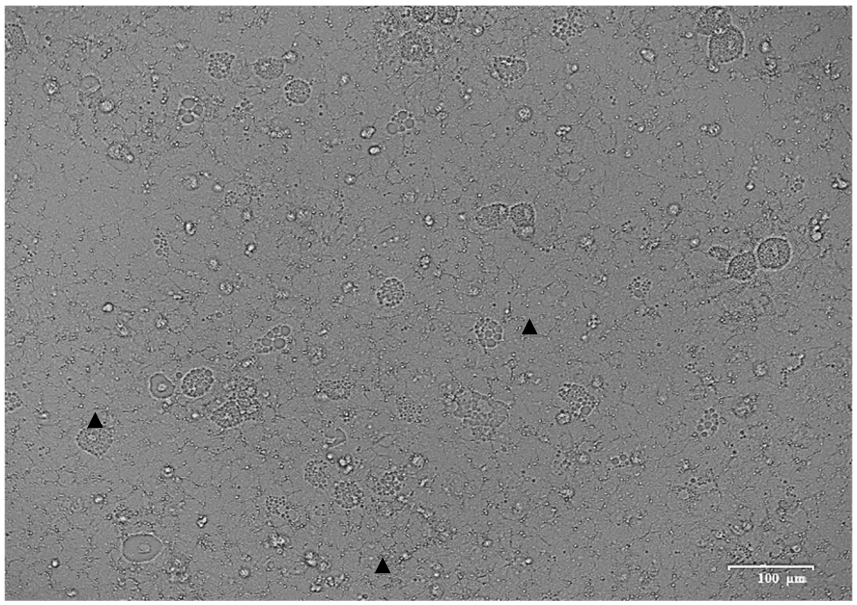

Figure 5. AML12 cells in high density in a T75 cell culture flask. Bright-field microscopy images of AML12 cells 48h after passage were taken in a 20x amplification in a ZOE Fluorescent Cell Imager (Bio-Rad Laboratories, Hercules, California, United States). Arrowheads indicate areas with regular cell morphology. This image is representative of 2 independent experiments. The scale bar is equivalent to 100 µm.

The next step was characterising these cells' growth by obtaining their growth curve. This would allow us to determine the optimal time to conduct any experiments. To do so, Sulforhodamine B (SBR) colourimetric assays were performed.

This technique allows an evaluation of cell growth by directly quantifying total protein mass, which directly correlates with cell mass (120). Since this assay does not rely on determining the metabolic function or activity of living cells, it eliminates the influence of varying biological parameters, such as increased metabolic rate or variations in mitochondrial activity, which could differ in the various independent assays (121). The theoretical premise behind this assay, as shown in Figure 6, is that the SRB dye, a bright pink amino xanthene dye with two sulfonic groups, can bind to basic amino acids under mildly acidic conditions and dissociate under basic conditions. The binding of the SBR dye is stoichiometric, so the amount of dye extracted from stained cells is directly proportional to the cell mass (122). This assay has advantages such as its low cost, good linearity and high sensitivity (121).

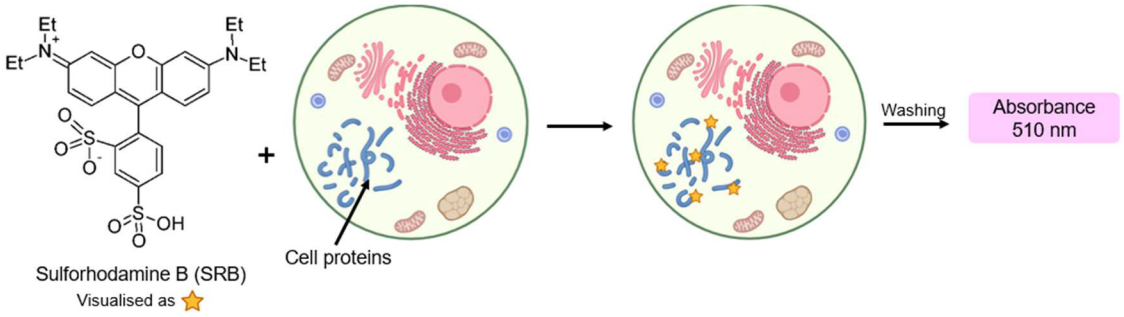

Figure 6. Structural formula of Sulforhodamine B and schematic depiction of an SRB colorimetric assay. Briefly, the SRB dye can bind to basic amino acids, allowing for a colourimetric evaluation of total cellular protein by reading the absorbance at 510 nm. This value directly correlates with cell number. Image created with BioRender.

Two different cell platting densities were tested for this assay: $1x10^5$ cells/mL and $2.5x10^5$ cells/mL. The obtained results are depicted in Figure 7. Building upon this result, we opted to conduct experiments using the higher cell density 24 hours after seeding since, at this time point, the cells had not only adhered to the plates but also already displayed their typical morphology. Additionally, if the cells were to be platted at this time point, they could be kept for an extra 48 hours without reaching the stationary growth phase.

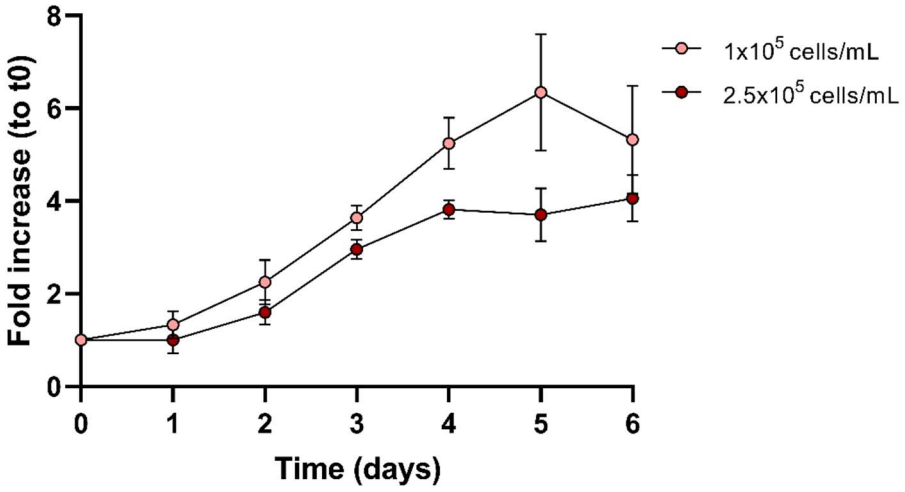

Figure 7. Graphical representation of AML12 cell growth curve. Cells were kept for seven days post-seeding, and the SRB colourimetric assay was performed for each time point indicated. Data are expressed as the fold increase relative to t0 (0 hours post-seeding). The graph represents the average ± SD of three independent experiments with triplicates.

Furthermore, it is essential to mention that these cells have to be seeded in pre-coated plates since they display attachment issues in non-coated plates. Despite adhering to the bottom of the wells just a few hours after seeding, after 24 hours, they stopped adhering and formed aggregates in suspension. This obstacle was overcome by coating the plates with either gelatine or collagen. At first, we used gelatine. Although cells adhered normally to it, gelatine displayed autofluorescence, which was incompatible with follow-up cell viability assays, described in the following section. As such, we switched to collagen-coated plates, which allowed these cells to adhere properly and display their typical morphology.

2. Viability Assays

2.1. Optimisation

The next step in this project was to conduct AML12 viability assays. To do that, we conducted resazurin assays, which were first optimised for this cell line.

Resazurin assays are widely used to determine cellular viability in prokaryotic and eukaryotic cells. Resazurin is a blue, low-fluorescence compound that enters cells and is metabolised by viable cells with an active metabolism into resorufin, a pink, highly fluorescent compound (Figure 8). Because of this, the resorufin fluorescence output is directly proportional to the number of metabolically active and viable cells (123).

Alongside its advantages, such as simplicity, reproducibility, sensitivity, and low cost (124), this assay is also non-destructive. It does not lead to cell lysis, allowing the same set of cells to be used in further tests or measurements (125). Regardless of the advantages listed, attention should be raised to the fact that resazurin can be intrinsically toxic for particular cell types (126), so these assays should be conducted cautiously.

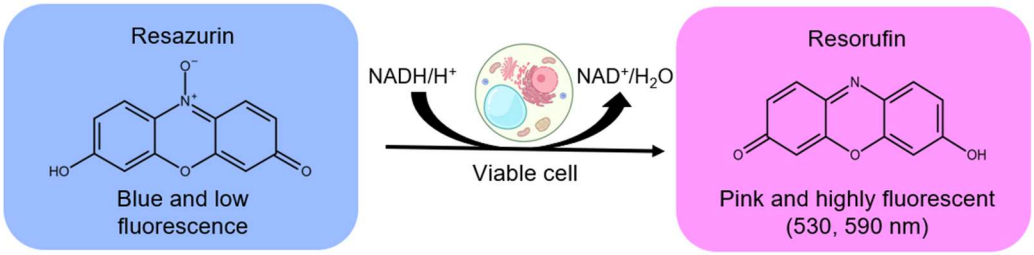

Figure 8. Schematic depiction of a resazurin assay alongside the structural formula of both resazurin and resorufin. Reduction of resazurin and formation of resorufin product. Resazurin, a low-fluorescence dye with a blue colour, is converted to resorufin, a pink, fluorescent product whose fluorescence can be read using an excitation wavelength of 530 nm and emission wavelength of 590 nm. The obtained value directly correlates with cell viability. Image created with BioRender.

To proceed with the assay optimisation, we tested the same two cell platting densities (1x10^5 cells/mL and 2.5x10^5 cells/mL) as before, incubated with increasing resazurin concentrations (0.25, 0.50, 1.00, 1.25, 1.50 and 2.00 mM) for 6 hours (Figure 9).

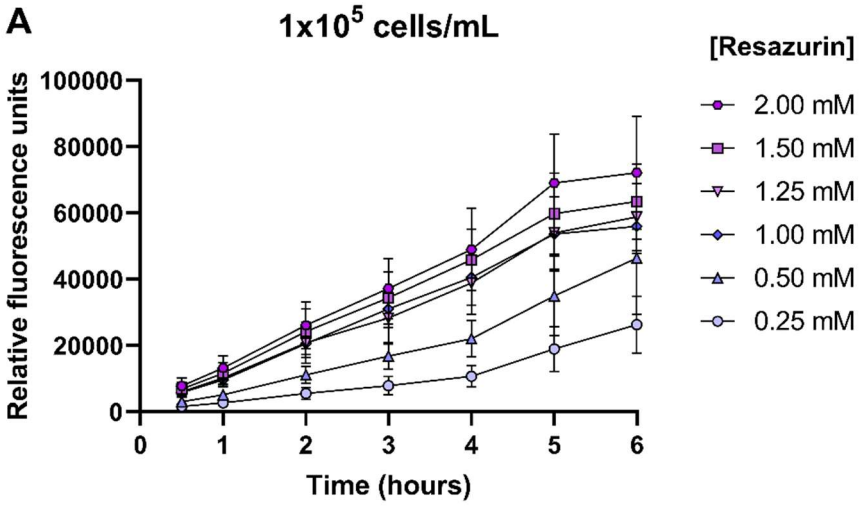

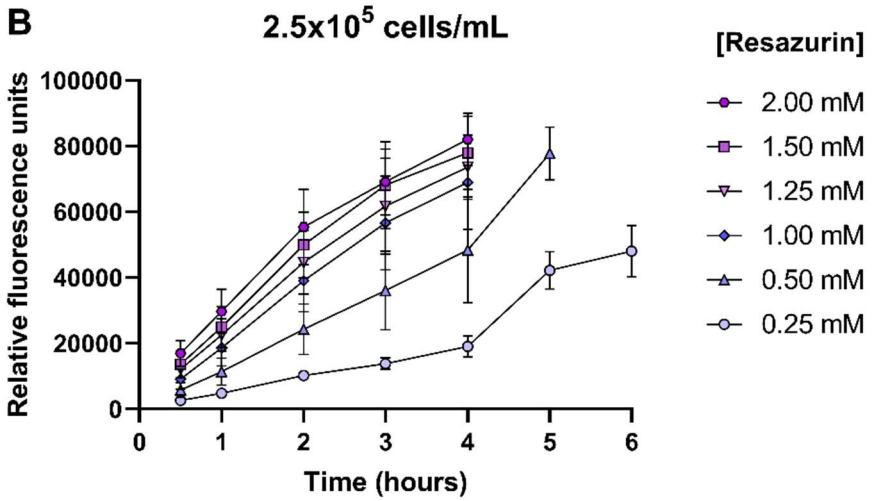

Figure 9. Graphical representation of the resazurin assay optimisation. Two different cell platting densities were tested, A – $1x10^5$ cells/mL and B – $2.5x10^5$ cells/mL with increasing resazurin concentrations. Cells were kept for 6 hours after resazurin application, and for each of the time points indicated, the resazurin signal was measured. Data are expressed as the average ± SD of four independent experiments with triplicates.

Based on the results depicted in Figure 9 and Figure S1, we opted to use the higher cell density. This choice was based on the fact that, for higher cell densities at the same concentration and time point, there was a higher resazurin signal, which is easier to read because of higher signal specificity. Higher resazurin concentrations also lead to a higher resazurin output signal. However, the resazurin concentration should be as low as possible due to its potential toxicity. With this in mind, the resazurin concentration chosen was 1.25 mM since it was more of an intermediate concentration, but obtaining a good resazurin output was already possible. We also decided to measure resazurin output 2 hours after this compound had been applied since, after this time, some of the wells already displayed an overflow signal, and we wanted the assays to be as reproducible as possible.

2.2. BMM-Conditioned Medium Impacts AML12 Cell Viability

After optimising the resazurin assay, we used this tool to start studying the communication between hepatocytes and macrophages. We wanted to assess whether infected or non-infected BMMs could impact AML12 viability, so we treated AML12 cells with BMM-conditioned media, as depicted in Figure 10.

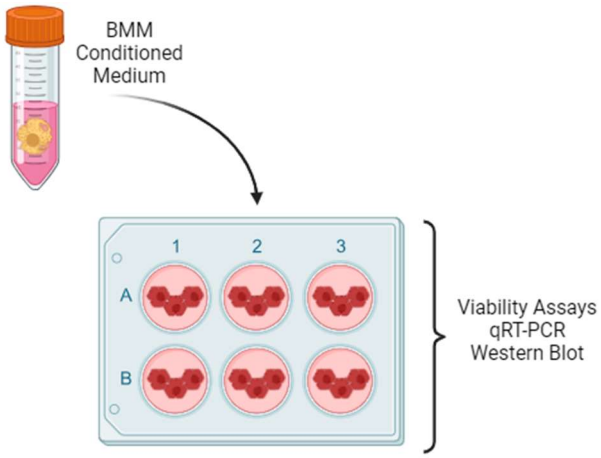

Figure 10. Schematic representation of the experimental design used. AML12 cells platted in 6-well plates were treated with BMM-conditioned media. Following this, viability assays, qRT-PCR or western blot analysis were performed. Image created with BioRender.

The conditioned media came from non-infected or infected BMMs kept in culture for 48, 72, or 96 hours post-infection. To evaluate the infection progression in BMMs, bacteria were quantified at each time point mentioned above. The results obtained are represented in Figure 11. It shows that the bacterial load increased by approximately 0.2 log units every 24 hours after the initial 48 hours PI.

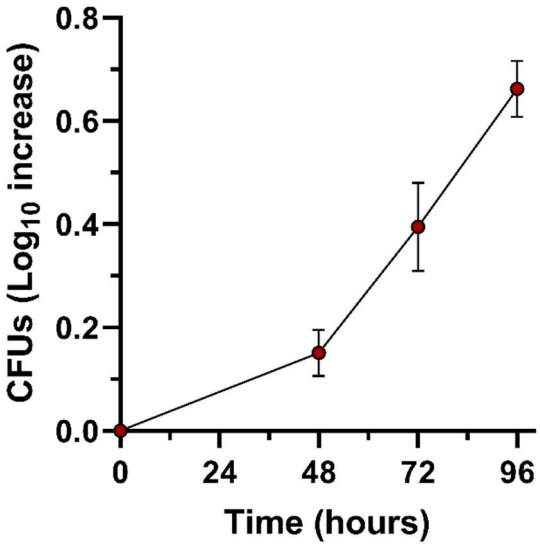

Figure 11. Graphical representation of the bacterial load of infected BMMs. BMMs were infected with *M. avium* 25291, and bacteria were quantified by a CFU assay. The graph shows the average ± SD of quadruplicates and is representative of 2 independent experiments. Data are expressed as Log_{10} increase, which corresponds to the difference between the Log_{10} of intramacrophagic mycobacteria CFUs/ mL in each time point (48, 72, and 96 hours PI) and the Log_{10} of intramacrophagic mycobacteria CFUs/ mL for t0.

Figure 12 depicts the results obtained for the viability assays. The signal was measured 48 hours after the contact between the AML12 cells and the conditioned media, and this was maintained for all the experiments conducted.

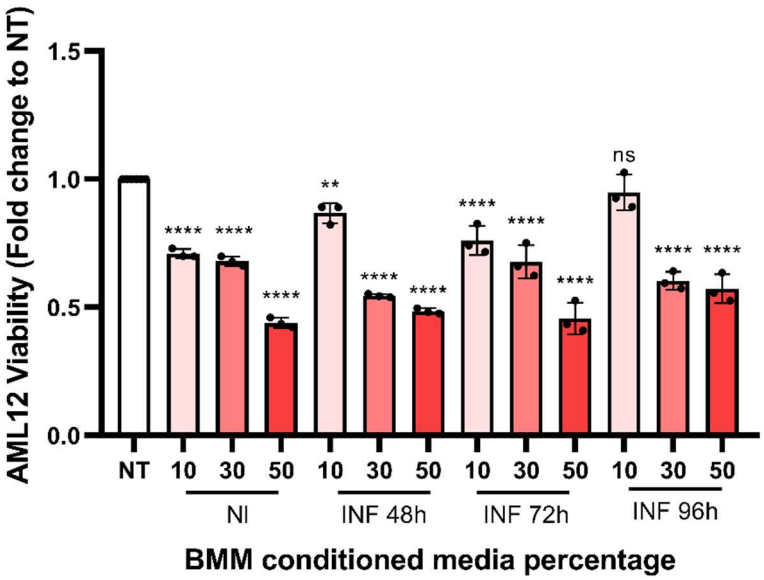

Figure 12. Graphical representation of AML12 viability in the presence of BMM conditioned media from Non-Infected (NI) and Infected (INF) BMMs in increasing percentages of volume (10, 30 or 50%). Cell media were substituted (according to the different percentages) 24 hours after cell seeding and were kept for another 48 hours afterwards. The resorufin signal was read 2 hours after resazurin application. Data are expressed as the fold change relative to Non-Treated (NT) cells. The graph represents the average ± SD of three independent experiments with triplicates. Statistics: ordinary one-way ANOVA. **p< 0.01, ***p< 0.001, ****p<0.0001, when comparing the experimental groups with non-treated cells.

AML 12's viability was reduced to approximately 70.90 ± 0.02 % in the presence of only 10% of non-infected BMM-conditioned medium. The viability reduction increased as the percentage of BMM-conditioned medium also increased. When AML 12 cells were cultured in the presence of 50% of BMM-conditioned medium, the viability reached a value of 43.86 ± 0.02 %. The same trend was visible for both conditioned media originating from infected or non-infected BMMs.

Thus, BMM-conditioned media decreased hepatocyte viability dose-dependently. Additionally, this effect seemed to be independent of whether the macrophages were infected since there was no significant difference between infected and non-infected BMM-conditioned media.

2.3. AML12 Decreased Cell Viability in the Presence of BMM-Conditioned Media is Independent of Cell Medium Components

Although the previous results suggested that macrophages produce something that impacts AML12's viability, it is important to note that BMMs and AML12 have different cell medium requirements. While BMMs require conventional DMEM, AML12 cells use DMEM F12.

This led us to formulate different hypotheses for the viability reduction witnessed. Either DMEM is not adequate to support AML12's survival and growth; macrophages consume part of DMEM's nutrients, which is why BMM-conditioned media do not support AML 12 cells' survival and growth; or macrophages produce and excrete toxic compounds, which decrease AML 12's survival and growth.

To test the first hypothesis, we conducted the same essays, but this time, we used different percentages of normal fresh DMEM in the AML12 cells. We can see that the same percentages used in the previous assays do not significantly impact AML12's viability; only when these cells were given only DMEM (100%) was their viability significantly hindered, being reduced to 40,18 ± 0.08 % (Figure 13).

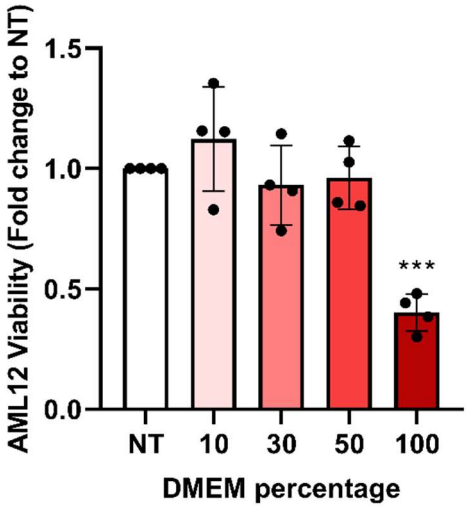

Figure 13. Graphical representation of AML12 viability in the presence of normal DMEM in increasing percentages. Cell media were substituted (according to the different percentages) 24 hours after cell seeding and were kept for another 48 hours afterwards. The resorufin signal was read 2 hours after resazurin application. Data are expressed as the fold change relative to non-treated (NT) cells. The graph represents the average ± SD of three independent experiments with triplicates. Statistics: ordinary one-way ANOVA. ***p< 0.001 when comparing the experimental groups with non-treated cells.

Furthermore, we wanted to confirm if the viability decrease was not due to the absence of nutrients that the BMMs had consumed. As such, we wanted to analyse how nutrient deprivation would affect the AML12 cells. Hence, we conducted a similar assay as the ones carried out previously, but this time, we used different percentages of PBS or old AML12-conditioned media as a media depleted in nutrients (Figure 14).

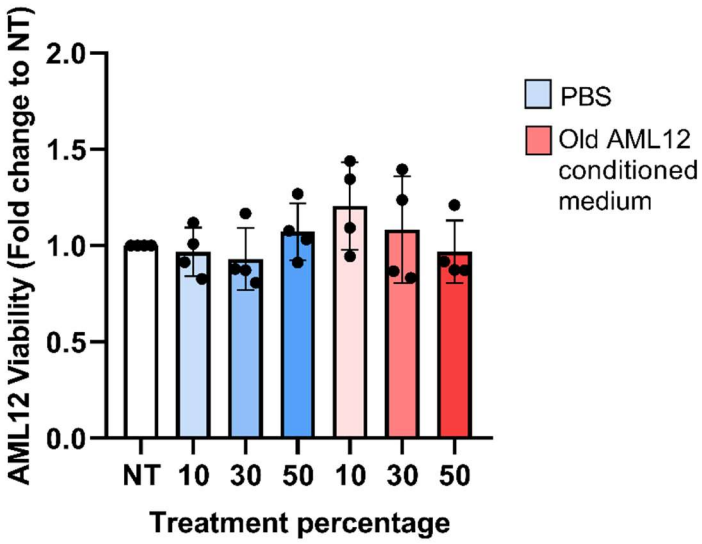

Figure 14. Graphical representation of AML12 viability in the presence of either PBS or old AML12 conditioned medium in increasing percentages. Cell media were substituted (according to the different percentages) 24 hours after cell seeding and were kept for another 48 hours afterwards. The resorufin signal was read 2 hours after resazurin application. Data are expressed as the fold change relative to Non-Treated (NT) cells. The graph represents the average ± SD of four independent experiments with triplicates. Statistics: ordinary one-way ANOVA.

With this assay, we could see that nutrient deprivation does not significantly impact AML12 viability. So, we confirmed that the effect of BMM-conditioned media could be due to some components that BMMs produce.

2.4. AML12 Cells Survive in the Presence of Exogenous Iron

With the previous results, we concluded that AML12 cells' viability is likely negatively impacted by BMM-conditioned medium and is not significantly hindered by factors such as differences in culture media and nutrient deprivation. Considering this, we wanted to test how a more drastic stimulus, such as iron overload, would affect these cells. To achieve this, we treated these cells with Ferric Ammonium Citrate (FAC).

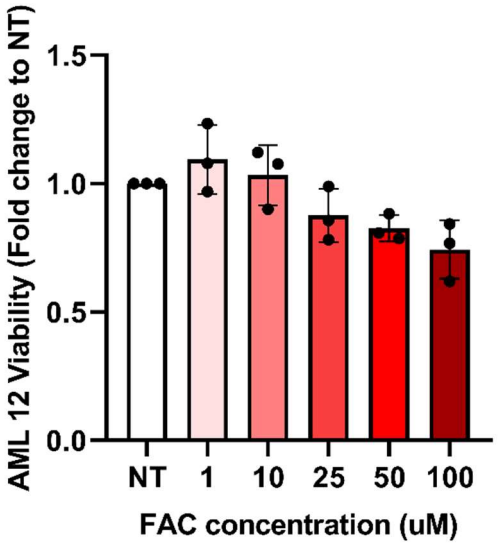

Figure 15. Graphical representation of AML12 viability in the presence of FAC in increasing concentrations (1, 10, 25, 50 and 100 µM). Cells were treated 24 hours after seeding and kept for another 48 hours. The resazurin signal was read 2 hours after its application. Data are expressed as the fold change relative to non-treated (NT) cells. The graph represents the average ± SD of four independent experiments with triplicates. Statistics: ordinary one-way ANOVA.

We can see that the toxic effect increased slightly in a dose-dependent manner. However, these FAC concentrations didn't significantly impact cell viability (Figure 15), although the intracellular iron levels clearly increased (from 45.46 to 248.6 µg/L), as confirmed by atomic absorption spectrometry (Figure S2).

Since these cells seem to be very resistant overall, this also gives us an additional hint that something that the BMMs are producing is triggering the decrease in cell viability. In light of this, the next step in this project was to investigate how these cells communicate.

3. How Do AML12 Cells and Macrophages Communicate?

3.1. Cytokine Analysis

With the previous results in mind, we inferred that something produced by the BMMs was impacting AML12's viability, and thus, we wanted to understand what this could be. Subsequently, we used a Bio-Plex Multiplex Immunoassay System (Bio-Rad Laboratories, Hercules, California, United States), which allows the user to analyse a cluster of multiple cytokines simultaneously. The panel chosen for this work included the following analytes: IFN-γ, IL-1β, IL-6, IL-10, IL-17A and TNF-α. The significant advantage

of this assay, when compared to conventional ELISA assays, relies on the fact that it is possible to analyse several analytes simultaneously, which is both timesaving and requires a smaller amount of sample to be analysed.

In this assay, we analysed conditioned media from Non-Infected and Infected BMMs (48, 72, and 96h PI) and supernatants of AML12 cultured with the BMM-conditioned medium. Unfavourably, all the obtained results were below the assay's detection limit. Notwithstanding, the analysed cytokines could still be present in the samples, just in minimal concentrations.

On that account, we decided to conduct an ELISA assay to assess the TNFα content in both NI and Infected BMMs (48, 72, and 96h PI) conditioned medium. The obtained results are portrayed in Figure 16.

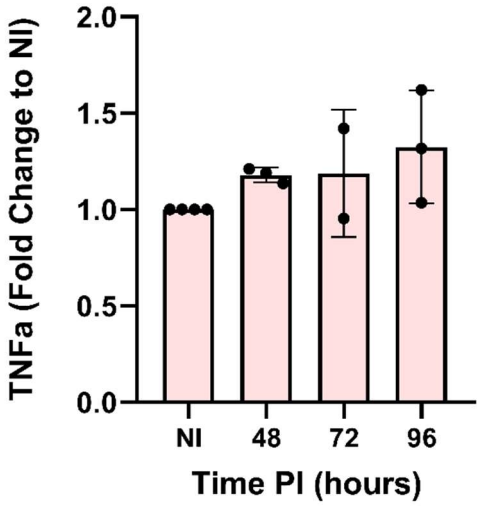

Figure 16. Graphical representation of TNF-α content in BMM conditioned medium. This analysis was conducted through ELISA. Data are expressed as the fold change relative to conditioned medium from Non-Infected (NI) BMMs. Each dot represents the average ± SD value of duplicates from 2-4 independent experiments. Statistics: ordinary one-way ANOVA.

Although there is no significant statistical difference in TNF-α content among the various samples, there appears to be an increasing tendency in this cytokine´s content as the infection progresses, which is approximately 30% higher at 96 hours PI compared to NI BMMs. This suggests that AML12 cells and BMMs may be communicating via cytokines. Afterwards, the next task was to understand the impact this communication had on the iron metabolism of AML12 cells.

4. AML12 Iron-Related Gene Expression is Affected by BMM-Conditioned Medium

Since the BMM-conditioned medium impacted AML12´s viability, we questioned whether that reduction in viability could be due to an effect on iron homeostasis. Therefore, we sought to evaluate the potential changes in AML12's iron-related transcriptome. To test this, we conducted qRT-PCR assays and analysed the following genes: *Hamp1*, *Ftl*, *Tf*, *Fth1, and Tfr1*. The experimental design used was the same as in Figure 10. AML12 cells were treated with 50% BMM conditioned medium and 50% DMEM F12. We based this choice on a pilot study (data not shown) in which we saw no significant difference in iron-related gene expression levels for cells treated with lower percentages (10% and 30%) of BMM-conditioned media compared to NT cells.

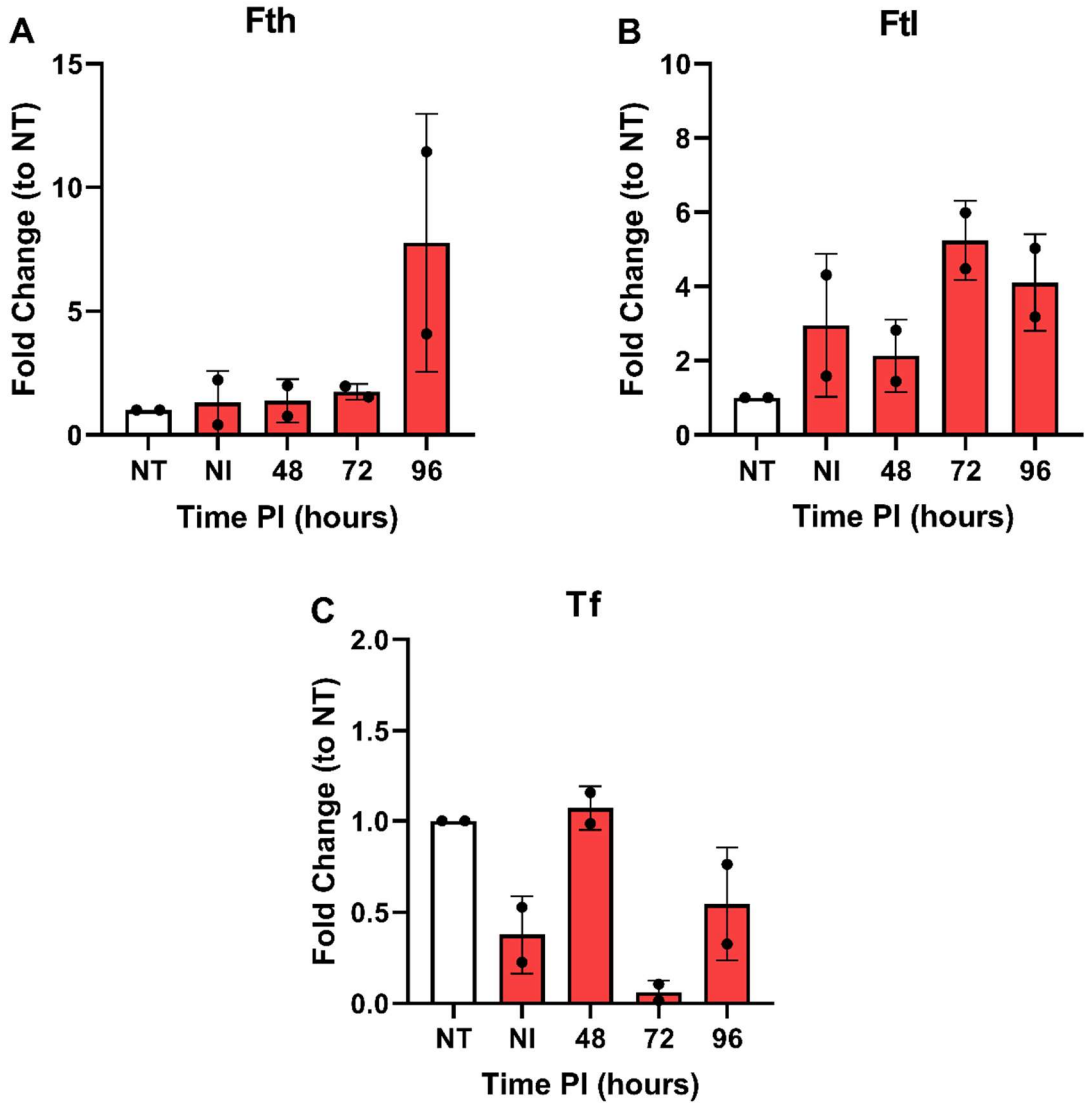

Figure 17. Graphical representation of RNA gene expression of **A** - *Fth*, **B** -*Ftl*, **C**- *Tf* in AML12 cells cultured with BMM-conditioned medium. This analysis was conducted through qRT-PCR. Cells were exposed 24 hours after seeding to 50% BMM-conditioned medium/ 50% DMEM F12 and kept for another 48 hours after. Data are expressed as the fold change relative to NT cells. The graph represents the average ± SD of two independent experiments conducted twice with duplicates. Statistics: ordinary one-way ANOVA.

Figure 17 portrays the obtained results. Although not statistically significant, the expression of *Fth* increased by approximately 7.7 times when AML 12 cells were cultured with medium from infected BMMs kept in culture for 96h (Figure 17A); however, it was not possible to draw a coherent conclusion about the changes in *Ftl* and *Tf* content (Figure 17B and C, respectively). Additionally, there was no amplification of the *Hamp1* and *Tfr1* genes.

5. AML12 Iron-Related Protein Expression is Affected by BMM-Conditioned Medium

In the same way that we investigated the possible effect of BMM-conditioned medium in the AML12's transcriptome, we wondered if the same tendencies were present in these cells' proteome, particularly regarding iron metabolism proteins. We also wanted to assess if obtaining any information about FTL, Tf, and TfR was possible since we couldn't detect any coherent changes with the qRT-PCR assays. Therefore, we conducted western blot assays for the following proteins: FTH, FTL, Tf, and TfR. The experimental design used was the same as in Figure 10. As in the previous assays, AML12 cells were treated with 50% BMM-conditioned medium and 50% DMEM F12.

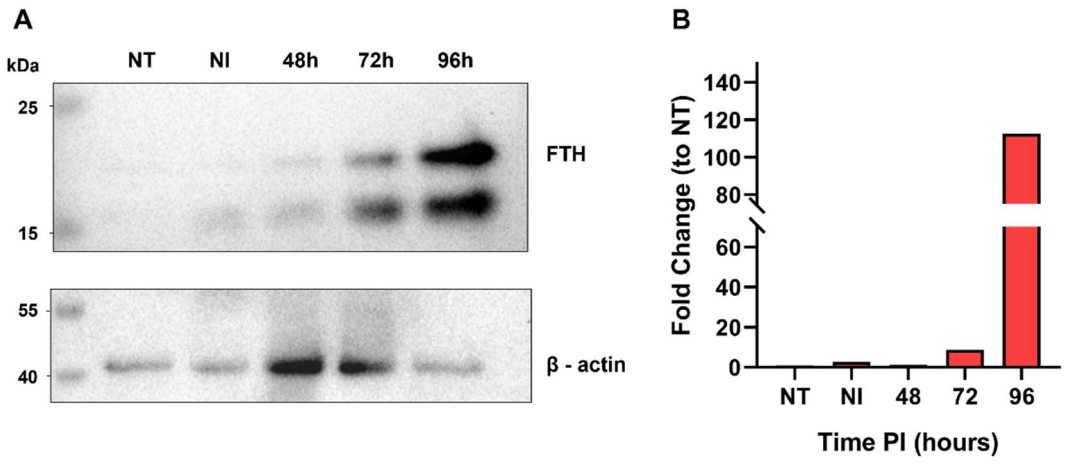

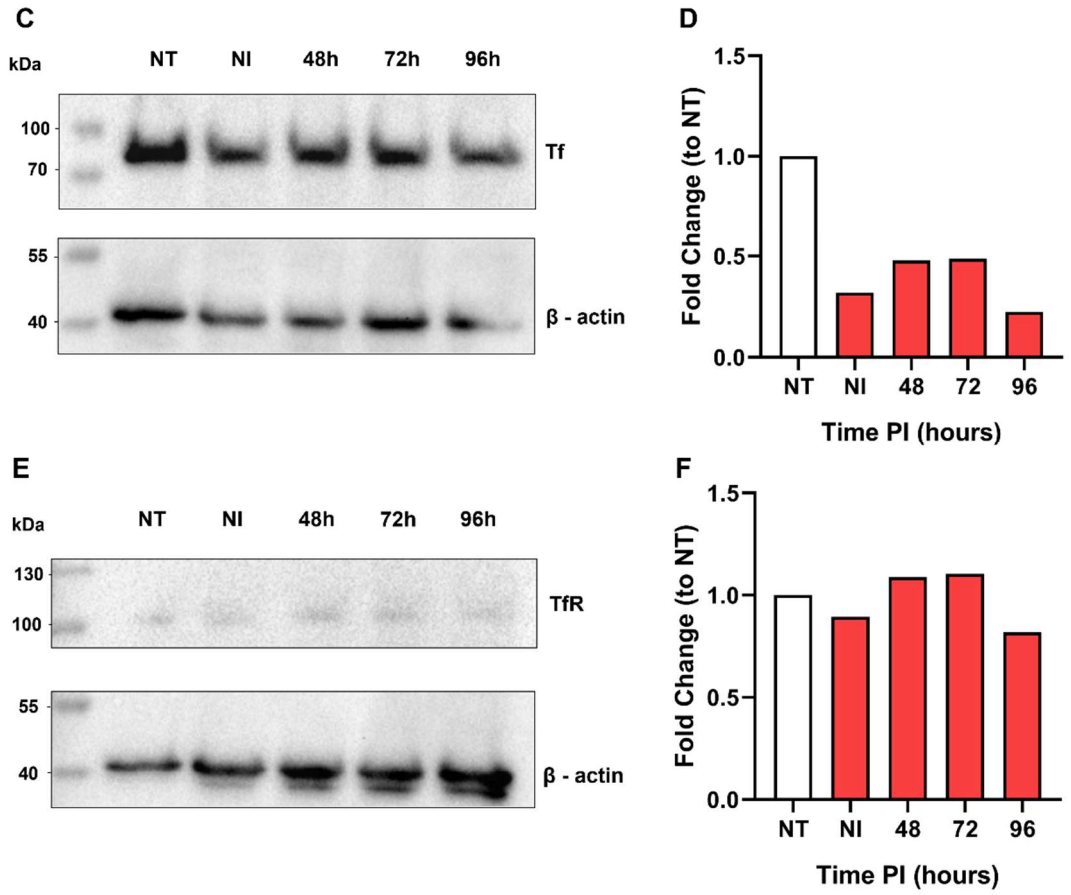

Figure 18. Protein expression of **A** – FTH, **C** – Tf, **E** – TfR in AML12 cells cultured with BMM-conditioned medium. Cells were exposed 24 hours after seeding to 50% BMM-conditioned medium/ 50% DMEM F12 and kept for another 48 hours after. This analysis was conducted through western blot. β-actin was used as the loading control. Protein quantification for FTH, Tf, and TfR are plotted in **B**, **D** and **F**, respectively. Data are expressed as the fold change relative to NT cells. The results are preliminary and represent one independent experiment.

Figure 18 portrays the results with their respective quantifications. Similarly, although these results are preliminary, there was an increase in FTH in AML12 treated with BMM-conditioned media throughout the infection, particularly in the 96-hour PI time point (Figures 18A and 18B). However, the levels of Tf and TfR remained relatively constant throughout the infection period. Additionally, it was not possible to assess the levels of FTL.

These results allowed us to conclude that BMM-conditioned medium affects not only AML12's viability but also its iron-related transcriptome and proteome.

IV – Discussion

This study sought to elucidate the mechanisms of iron-related communication between macrophages and hepatocytes during *M. avium* infection.

The central premise behind this project is based on a previous study that shows that, during *M. avium* infection, macrophages release FTH. This FTH impacts neighbouring hepatocyte cells regarding iron redistribution upon infection (24).

Although macrophagic and hepatocytic functions are well described separately, studies that address their communication are scarce, especially during infection. During this project, we established an in vitro model to mimic the possible paracrine communication between these cell types.

For the hepatocytic model, we used AML12 cells. This immortal cell line has been validated (110) and is widely used as a nontumorigenic hepatocytic model in several studies, including attempts to study the communication between these cells and macrophages (95, 127, 128) in different scenarios. As depicted in Figure 5, AML12 cells exhibit the typical flat, polygonal phenotype with granular cytoplasm characteristic of hepatocytes and do not display auto-fluorescence. We were able to establish this cell line in our laboratory following ATCC's instructions and in accordance with other researchers (95, 114).

We used BMMs for the macrophagic model not only because this cell model has been optimised and extensively used in our laboratory (115, 116) but also because it has been used in macrophage research in general (117, 129, 130). We cultured these cells, infected them with *M. avium*, and collected their conditioned medium. To confirm that the infection was successful, the progression of the infection was evaluated by determining the bacterial loads at each time point (48, 72 and 96 hours post-infection) (Figure 11). The obtained results are in accordance with pre-existing data that show the progression of *M. avium* infection in a BMM in vitro model (116, 131). This confirms that the infection was performed successfully.

We then used the BMM-conditioned medium to treat AML12 cells, as depicted in Figure 10. We conducted different experiments to investigate how this treatment impacted AML12 cells' viability, transcriptome, and proteome.

To carry out the viability assays, we started by implementing the resazurin protocol pre-existent in our laboratory that had been extensively used with BMMs.

However, we encountered several constrictions. The first was the fact that the AML12 cells were not able to adhere to the plates.

As aforementioned, primary hepatocytes need plates to be coated in either gelatine or collagen to adhere (84, 85). This can be explained by the need for their environment to resemble the liver extracellular matrix. With this in mind, we figured that AML12 cells might need a similar treatment.

Firstly, we started by seeding these cells in gelatine-coated plates since the primary hepatocyte protocol being tested in parallel to this thesis advised them to be seeded in that condition. It's also important to keep in mind the lower cost of gelatine compared to collagen. Despite gelatine-coated plates solving the adhering issues AML12 cells displayed, we could still not conduct resazurin assays; the signal would always overflow.

Finding this unusual, we analysed the platted cells under the fluorescence microscope. We discovered that gelatine had autofluorescence properties. This significantly interferes with measuring the resazurin signal, which is read at 530, 590 nm.

With this information in mind, we switched to using collagen-coated plates. These also allowed AML12 cells to adhere and did not display autofluorescence. Having solved this problem, we tried once again applying the resazurin protocol. Nonetheless, there was still a strong overflow signal when reading the resazurin signal. We suspected it could be due to incubation periods that were too long. In our pre-existent protocol, BMMs had to be incubated overnight with the resazurin solution to be possible to read their fluorescence signal. This could be explained by the fact that immortalised cell lines generally have a more active metabolism than primary cells (132). Because of this, we tested several incubation times, resazurin concentrations and cell platting densities to find the optimal ones (Figure 9 and S1).

After optimising the resazurin assays, we could start analysing how AML12 viability is impacted by BMM-conditioned medium. The results indicate that BMM-conditioned media significantly reduces AML12 cell viability in a dose-dependent manner, independent of whether the BMMs were infected with *M. avium* (Figure 12). Additionally, as shown by the control experiments with varying DMEM (Figure 13), PBS and old AML12-conditioned medium concentrations (Figure 14), this effect is not due to differences in the culture medium or nutrient deprivation. As such, these assays support the claim that macrophages release factors that negatively impact hepatocyte survival, regardless of whether they are infected or not.

Since these cells were resistant to the factors mentioned above, we wanted to assess how their viability would be affected by iron overload conditions. While iron deficiency anaemia is the most common symptom of disrupted iron homeostasis, certain haematological disorders are characterised by iron overload. Iron in plasma and cells is bound to proteins, keeping it redox-inactive. However, in cases of iron overload, a portion of iron becomes unbound (labile iron pool) and redox-active, producing excessive free radicals, which cause oxidative stress (133). The liver is considered one of the main organs affected by the oxidative stress caused by iron overload toxicity (134).

With this in mind and considering that the AML12 cells were resistant to differences in the culture medium and nutrient deprivation, we wanted to assess how iron overload could affect their viability. FAC was then used to mimic iron overload conditions. FAC is a relatively stable form of ferric citrate, a type of free iron that becomes more prevalent in blood during iron overload conditions (135).

The FAC concentrations chosen were similar to those used in previous experiments conducted in the group in BMMs (53). In that study, the FAC concentrations utilised were toxic for the BMMs and significantly decreased their viability.

A different study treated AML12 cells with FAC and evaluated its effect on insulin resistance and oxidative stress (135). Although iron overload affected the mentioned factors, cell viability was not assessed.

Figure 15 shows that although the toxic effect increases slightly as the FAC concentration doubles, the differences are not statistically significant. AML12's susceptibility to the toxicity of FAC is lower than BMMs' susceptibility. While both cell types are important in iron metabolism, hepatocytes handle a higher iron load due to the liver's role as the body's leading storage site for excess iron. This can explain AML12's lower susceptibility.

Altogether, we could conclude that these cells are highly resistant to adverse conditions. However, BMM-conditioned medium can significantly hinder their viability. With this, the next goal was to comprehend what the BMMs were producing that could lead to the viability effect we were observing.

Intercellular communication occurs through direct cell-cell contact, soluble factors such as cytokines and growth factors, and extracellular vesicles. These mechanisms work together to maintain homeostasis by adapting to stress conditions. However, dysregulation of any of these pathways can disrupt normal physiology and contribute to disease development.

Since our experimental model mimicked paracrine communication, we wanted to assess whether this communication could be mediated through cytokines. BMM proinflammatory cytokine release in the presence of stimuli, such as infection or LPS, has been extensively reported (53, 115, 136). With this in mind, we wanted to assess the presence of proinflammatory cytokines in BMM-conditioned medium.

Although the multiplex cytokine analysis yielded results below the detection limit, the subsequent ELISA assay for TNF-α revealed an increasing trend in this cytokine's content as the infection progressed (Figure 16).

Although this suggests that cytokines such as TNF-α may play a role in macrophage-hepatocyte communication, it is essential to keep in mind that the decrease in viability occurs regardless of BMM infection. Despite being a proinflammatory cytokine, analysing Figure 16, it is possible to see that its levels are very similar in the non-infected group. This could suggest that this cytokine is involved in the communication between these cell types. Notwithstanding, follow-up ELISA assays are needed to investigate if other cytokines may be involved.

Building upon this, we wondered if the BMM-conditioned medium could trigger any changes in AML12 cells' iron metabolism. To test this, we evaluated both the cell's transcriptome and proteome for important iron homeostasis components.

We decided to expose AML12 cells to 50% BMM-conditioned medium and 50% DMEM F12 since we saw no significant differences compared to non-treated cells for lower conditioned medium percentages (10% and 30%). Notwithstanding, with 50% BMM-conditioned medium, there is a significant reduction in AML12's viability. As a consequence, some of the effects we observed could be due to the loss of viability/ cell death. Likewise, conducting the PCR and western blot assays with the lower conditioned medium percentages would be necessary for comparison in the future.

Figure 17 shows that *Fth* content increases slightly through the infection period, being particularly high at 96 hours PI. Although both *Ftl* and *Tf* content are irregular, opposite tendencies were visualised. *Ftl* content is relatively constant throughout infection but is higher than in NT cells; the opposite is seen for *Tf* content. However, there is too much data variation to draw substantiated conclusions.

It is possible to speculate why there was no amplification of the *Hamp1* and *Tfr1* genes. The *Hamp1* gene encodes hepcidin. It would be expected, especially in an infection setting, for the levels of this hormone to be elevated. However, it has been shown in a study done in rat liver that, in the presence of a stimulus such as LPS, the

hepcidin mRNA levels peak at 6 and 36 hours after LPS treatment and diminish afterwards (137). A similar event could happen in this case. Since the signal was read 48 hours after the contact between the AML12 cells and the BMM-conditioned medium, it was not possible to detect any hepcidin mRNA levels.

Accordingly, in a study that also used AML12 cells, hepcidin mRNA levels were quantified 12 hours after the cells were given a stimulus. Moreover, in basal conditions, these cells also didn't show levels of hepcidin mRNA (138). As such, it would be relevant to try measuring hepcidin mRNA levels in a shorter period of time after exposing AML12 cells to BMM-conditioned medium.

The lack of *Tfr1* amplification could be explained by the fact that there are multiple forms of TfR, TfR1 and TfR2, and two alternatively spliced forms of TfR2 transcripts have been identified: TfR2α and TfR2β (139). Although TfR1 and TrR2 α's primary structures bear a significant resemblance, their mRNA is quite different (140). It has been shown that TfR2α is highly expressed not only in the human liver but also in HepG2 cells (141). Additionally, it has been found in K562 cells, an immortalised myelogenous leukaemia cell line, that iron chelation up-regulates TfR1 and down-regulates TfR2, and iron overload has the opposite effect (140). Additionally, considering that it was possible to detect TfR in the western blot (Figure 18 E, F) despite the low levels, it would be relevant to investigate AML12's *TfR2* mRNA levels.

In the same way that the levels of *Fth* mRNA peaked at 96 hours PI, the same tendency was observed for FTH protein levels (Figure 18 A, B). Here, we can see that there is a slight increase in the levels of this protein throughout the infection period and a higher increase in the last time point.

Likewise, similarly to the *Tf* mRNA levels, the levels of Tf were pretty constant throughout the infection time points but were lower than the levels of NT cells.

It is important to mention that the results obtained through western blot are only preliminary as they only represent one independent experiment. Also, the results obtained for FTL were omitted since there were many unspecific bands and too much background.

The results described align with the previously acquired data from the group, in which it was determined that the levels of FTH are elevated in the serum of infected mice despite its myeloid origin. Even though FTH, in this case, has a hepatic origin, it's an interesting parallelism that deserves further investigation, especially since there is communication between these cell types.

Furthermore, a different study reports an increase in the expression of FTH by both liver macrophages and hepatocytes in mice subjected to caecal ligation and puncture as a model of polymicrobial infection (142).

Altogether, the data obtained within this work suggest that BMM-conditioned medium impacts several parameters regarding AML12 cells' metabolism. With particular interest in iron metabolism.

Nevertheless, the model used is a rather simplistic model to mimic paracrine communication between cells. Although it served as a first approach to understanding the communication between hepatocytes and macrophages, in the future, it would be relevant to establish a more complex model to study paracrine communication and, later on, direct communication. As for a model of paracrine communication, co-cultures could be applied in a similar fashion as in Figure 4. It is a model that can more closely resemble physiological conditions as the macrophages and hepatocytes are constantly communicating with one another, although still indirectly. Additionally, it would be possible to better assess macrophages' effect on hepatocytes while simultaneously evaluating hepatocytes' effect on macrophages. As for a direct communication model, it would also be pertinent to establish a spheroid comprised of both hepatocytes and macrophages.

V – References

1. Huynh U, Zastrow ML. Metallobiology of Lactobacillaceae in the gut microbiome. J Inorg Biochem. 2023;238:112023.
2. Guengerich FP. Mechanisms of Cytochrome P450-Catalyzed Oxidations. ACS Catal. 2018;8(12):10964-76.
3. Hentze MW, Muckenthaler MU, Andrews NC. Balancing acts: molecular control of mammalian iron metabolism. Cell. 2004;117(3):285-97.
4. Muckenthaler MU, Rivella S, Hentze MW, Galy B. A Red Carpet for Iron Metabolism. Cell. 2017;168(3):344-61.
5. Ganz T, Nemeth E. Regulation of iron acquisition and iron distribution in mammals. Biochim Biophys Acta. 2006;1763(7):690-9.
6. Cappellini MD, Musallam KM, Taher AT. Iron deficiency anaemia revisited. J Intern Med. 2020;287(2):153-70.
7. Park E, Chung SW. ROS-mediated autophagy increases intracellular iron levels and ferroptosis by ferritin and transferrin receptor regulation. Cell Death Dis. 2019;10(11):822.
8. Kowalczyk P, Kaczynska K, Kleczkowska P, Bukowska-Osko I, Kramkowski K, Sulejczak D. The Lactoferrin Phenomenon-A Miracle Molecule. Molecules. 2022;27(9).
9. Hooda J, Shah A, Zhang L. Heme, an essential nutrient from dietary proteins, critically impacts diverse physiological and pathological processes. Nutrients. 2014;6(3):1080-102.
10. Drakesmith H, Prentice AM. Hepcidin and the iron-infection axis. Science. 2012;338(6108):768-72.
11. Hentze MW, Muckenthaler MU, Galy B, Camaschella C. Two to tango: regulation of Mammalian iron metabolism. Cell. 2010;142(1):24-38.
12. Gomes AC, Moreira AC, Mesquita G, Gomes MS. Modulation of Iron Metabolism in Response to Infection: Twists for All Tastes. Pharmaceuticals (Basel). 2018;11(3).
13. Galy B, Ferring-Appel D, Becker C, Gretz N, Grone HJ, Schumann K, et al. Iron regulatory proteins control a mucosal block to intestinal iron absorption. Cell Rep. 2013;3(3):844-57.
14. Das NK, Schwartz AJ, Barthel G, Inohara N, Liu Q, Sankar A, et al. Microbial Metabolite Signaling Is Required for Systemic Iron Homeostasis. Cell Metab. 2020;31(1):115-30 e6.
15. Ganz T. Macrophages and Iron Metabolism. Microbiol Spectr. 2016;4(5).

16. Theil EC. Ferritin: structure, gene regulation, and cellular function in animals, plants, and microorganisms. Annu Rev Biochem. 1987;56:289-315.
17. Moreira AC, Mesquita G, Gomes MS. Ferritin: An Inflammatory Player Keeping Iron at the Core of Pathogen-Host Interactions. Microorganisms. 2020;8(4).
18. Recalcati S, Invernizzi P, Arosio P, Cairo G. New functions for an iron storage protein: the role of ferritin in immunity and autoimmunity. J Autoimmun. 2008;30(1-2):84-9.
19. Cheepsunthorn P, Palmer C, Connor JR. Cellular distribution of ferritin subunits in postnatal rat brain. J Comp Neurol. 1998;400(1):73-86.
20. Cai CX, Birk DE, Linsenmayer TF. Ferritin is a developmentally regulated nuclear protein of avian corneal epithelial cells. J Biol Chem. 1997;272(19):12831-9.
21. Levi S, Corsi B, Bosisio M, Invernizzi R, Volz A, Sanford D, et al. A human mitochondrial ferritin encoded by an intronless gene. J Biol Chem. 2001;276(27):24437-40.
22. Wang W, Knovich MA, Coffman LG, Torti FM, Torti SV. Serum ferritin: Past, present and future. Biochim Biophys Acta. 2010;1800(8):760-9.
23. Arosio P, Adelman TG, Drysdale JW. On ferritin heterogeneity. Further evidence for heteropolymers. J Biol Chem. 1978;253(12):4451-8.
24. Moreira AC, Silva T, Mesquita G, Gomes AC, Bento CM, Neves JV, et al. H-Ferritin Produced by Myeloid Cells Is Released to the Circulation and Plays a Major Role in Liver Iron Distribution during Infection. Int J Mol Sci. 2021;23(1).
25. Mehlenbacher M, Poli M, Arosio P, Santambrogio P, Levi S, Chasteen ND, et al. Iron Oxidation and Core Formation in Recombinant Heteropolymeric Human Ferritins. Biochemistry-Us. 2017;56(30):3900-12.
26. Luscieti S, Santambrogio P, Langlois d'Estaintot B, Granier T, Cozzi A, Poli M, et al. Mutant ferritin L-chains that cause neurodegeneration act in a dominant-negative manner to reduce ferritin iron incorporation. J Biol Chem. 2010;285(16):11948-57.
27. Park CH, Valore EV, Waring AJ, Ganz T. Hepcidin, a urinary antimicrobial peptide synthesized in the liver. J Biol Chem. 2001;276(11):7806-10.
28. Krause A, Neitz S, Magert HJ, Schulz A, Forssmann WG, Schulz-Knappe P, et al. LEAP-1, a novel highly disulfide-bonded human peptide, exhibits antimicrobial activity. FEBS Lett. 2000;480(2-3):147-50.
29. Zhou Z, Xu MJ, Gao B. Hepatocytes: a key cell type for innate immunity. Cell Mol Immunol. 2016;13(3):301-15.

30. Schwartz AJ, Das NK, Ramakrishnan SK, Jain C, Jurkovic MT, Wu J, et al. Hepatic hepcidin/intestinal HIF-2alpha axis maintains iron absorption during iron deficiency and overload. J Clin Invest. 2019;129(1):336-48.

31. Rishi G, Subramaniam VN. The liver in regulation of iron homeostasis. Am J Physiol Gastrointest Liver Physiol. 2017;313(3):G157-G65.

32. Camaschella C, Nai A, Silvestri L. Iron metabolism and iron disorders revisited in the hepcidin era. Haematologica. 2020;105(2):260-72.

33. Nemeth E, Tuttle MS, Powelson J, Vaughn MB, Donovan A, Ward DM, et al. Hepcidin regulates cellular iron efflux by binding to ferroportin and inducing its internalization. Science. 2004;306(5704):2090-3.

34. Drakesmith H, Nemeth E, Ganz T. Ironing out Ferroportin. Cell Metab. 2015;22(5):777-87.

35. Ganz T. Hepcidin in iron metabolism. Curr Opin Hematol. 2004;11(4):251-4.

36. Singh B, Arora S, Agrawal P, Gupta SK. Hepcidin: a novel peptide hormone regulating iron metabolism. Clin Chim Acta. 2011;412(11-12):823-30.

37. D'Angelo G. Role of hepcidin in the pathophysiology and diagnosis of anemia. Blood Res. 2013;48(1):10-5.

38. Nicolas G, Chauvet C, Viatte L, Danan JL, Bigard X, Devaux I, et al. The gene encoding the iron regulatory peptide hepcidin is regulated by anemia, hypoxia, and inflammation. J Clin Invest. 2002;110(7):1037-44.

39. Wilkinson N, Pantopoulos K. The IRP/IRE system in vivo: insights from mouse models. Front Pharmacol. 2014;5:176.

40. Docherty KF, Welsh P, Verma S, De Boer RA, O'Meara E, Bengtsson O, et al. Iron Deficiency in Heart Failure and Effect of Dapagliflozin: Findings From DAPA-HF. Circulation. 2022;146(13):980-94.

41. Porter JB, El-Alfy M, Viprakasit V, Giraudier S, Chan LL, Lai Y, et al. Utility of labile plasma iron and transferrin saturation in addition to serum ferritin as iron overload markers in different underlying anemias before and after deferasirox treatment. Eur J Haematol. 2016;96(1):19-26.

42. Ohgami RS, Campagna DR, Greer EL, Antiochos B, McDonald A, Chen J, et al. Identification of a ferrireductase required for efficient transferrin-dependent iron uptake in erythroid cells. Nat Genet. 2005;37(11):1264-9.

43. Chitambar CR, Wereley JP. Transferrin receptor-dependent and -independent iron transport in gallium-resistant human lymphoid leukemic cells. Blood. 1998;91(12):4686-93.

44. Kotamraju S, Chitambar CR, Kalivendi SV, Joseph J, Kalyanaraman B. Transferrin receptor-dependent iron uptake is responsible for doxorubicin-mediated apoptosis in endothelial cells: role of oxidant-induced iron signaling in apoptosis. J Biol Chem. 2002;277(19):17179-87.

45. Trinder D, Zak O, Aisen P. Transferrin receptor-independent uptake of differic transferrin by human hepatoma cells with antisense inhibition of receptor expression. Hepatology. 1996;23(6):1512-20.

46. Page MGP. The Role of Iron and Siderophores in Infection, and the Development of Siderophore Antibiotics. Clin Infect Dis. 2019;69(Suppl 7):S529-S37.

47. Silva-Gomes S, Vale-Costa S, Appelberg R, Gomes MS. Iron in intracellular infection: to provide or to deprive? Front Cell Infect Microbiol. 2013;3:96.

48. Golonka R, Yeoh BS, Vijay-Kumar M. The Iron Tug-of-War between Bacterial Siderophores and Innate Immunity. J Innate Immun. 2019;11(3):249-62.

49. Moreira AC, Neves JV, Silva T, Oliveira P, Gomes MS, Rodrigues PN. Hepcidin-(In)dependent Mechanisms of Iron Metabolism Regulation during Infection by Listeria and Salmonella. Infect Immun. 2017;85(9).

50. Silva-Gomes S, Bouton C, Silva T, Santambrogio P, Rodrigues P, Appelberg R, et al. Mycobacterium avium infection induces H-ferritin expression in mouse primary macrophages by activating Toll-like receptor 2. PLoS One. 2013;8(12):e82874.

51. Torti FM, Torti SV. Regulation of ferritin genes and protein. Blood. 2002;99(10):3505-16.

52. To K, Cao R, Yegiazaryan A, Owens J, Venketaraman V. General Overview of Nontuberculous Mycobacteria Opportunistic Pathogens: Mycobacterium avium and Mycobacterium abscessus. J Clin Med. 2020;9(8).

53. Mesquita G, Silva T, Gomes AC, Oliveira PF, Alves MG, Fernandes R, et al. H-Ferritin is essential for macrophages' capacity to store or detoxify exogenously added iron. Sci Rep. 2020;10(1):3061.

54. Bhatia SN, Underhill GH, Zaret KS, Fox IJ. Cell and tissue engineering for liver disease. Sci Transl Med. 2014;6(245):245sr2.

55. Berasain C, Avila MA. Regulation of hepatocyte identity and quiescence. Cell Mol Life Sci. 2015;72(20):3831-51.

56. Moradi E, Jalili-Firoozinezhad S, Solati-Hashjin M. Microfluidic organ-on-a-chip models of human liver tissue. Acta Biomater. 2020;116:67-83.

57. Ma Y, Hu L, Tang J, Guo W, Feng Y, Liu Y, et al. Three-Dimensional Cell Co-Culture Liver Models and Their Applications in Pharmaceutical Research. Int J Mol Sci. 2023;24(7).

58. Rincon M. Interleukin-6: from an inflammatory marker to a target for inflammatory diseases. Trends Immunol. 2012;33(11):571-7.
59. Calabrese LH, Rose-John S. IL-6 biology: implications for clinical targeting in rheumatic disease. Nat Rev Rheumatol. 2014;10(12):720-7.
60. Norris CA, He M, Kang LI, Ding MQ, Radder JE, Haynes MM, et al. Correction: Synthesis of IL-6 by Hepatocytes Is a Normal Response to Common Hepatic Stimuli. Plos One. 2019;14(10):e0224498.
61. Zakin MM. Regulation of transferrin gene expression. FASEB J. 1992;6(14):3253-8.
62. Thiagarajan P, Parker CJ, Prchal JT. How Do Red Blood Cells Die? Front Physiol. 2021;12:655393.
63. Chow A, Huggins M, Ahmed J, Hashimoto D, Lucas D, Kunisaki Y, et al. CD169(+) macrophages provide a niche promoting erythropoiesis under homeostasis and stress. Nat Med. 2013;19(4):429-36.
64. Manwani D, Bieker JJ. The erythroblastic island. Curr Top Dev Biol. 2008;82:23-53.
65. Davies LC, Jenkins SJ, Allen JE, Taylor PR. Tissue-resident macrophages. Nat Immunol. 2013;14(10):986-95.
66. Zigmond E, Jung S. Intestinal macrophages: well educated exceptions from the rule. Trends Immunol. 2013;34(4):162-8.
67. Kondo H, Saito K, Grasso JP, Aisen P. Iron metabolism in the erythrophagocytosing Kupffer cell. Hepatology. 1988;8(1):32-8.
68. Leimberg MJ, Prus E, Konijn AM, Fibach E. Macrophages function as a ferritin iron source for cultured human erythroid precursors. J Cell Biochem. 2008;103(4):1211-8.
69. Soares MP, Hamza I. Macrophages and Iron Metabolism. Immunity. 2016;44(3):492-504.
70. Parrow NL, Fleming RE, Minnick MF. Sequestration and scavenging of iron in infection. Infect Immun. 2013;81(10):3503-14.
71. Gomes-Pereira S, Rodrigues PN, Appelberg R, Gomes MS. Increased susceptibility to Mycobacterium avium in hemochromatosis protein HFE-deficient mice. Infect Immun. 2008;76(10):4713-9.
72. Willebrords J, Crespo Yanguas S, Maes M, Decrock E, Wang N, Leybaert L, et al. Structure, Regulation and Function of Gap Junctions in Liver. Cell Commun Adhes. 2015;22(2-6):29-37.

73. Al Amir Dache Z, Thierry AR. Mitochondria-derived cell-to-cell communication. Cell Rep. 2023;42(7):112728.

74. Paschos NK, Brown WE, Eswaramoorthy R, Hu JC, Athanasiou KA. Advances in tissue engineering through stem cell-based co-culture. J Tissue Eng Regen Med. 2015;9(5):488-503.

75. Padberg F, Hoper T, Henkel S, Driesch D, Luch A, Zellmer S. Novel indirect co-culture of immortalised hepatocytes with monocyte derived macrophages is characterised by pro-inflammatory cytokine networks. Toxicol In Vitro. 2021;73:105134.

76. Rodrigues PN, Gomes SS, Neves JV, Gomes-Pereira S, Correia-Neves M, Nunes-Alves C, et al. Mycobacteria-induced anaemia revisited: a molecular approach reveals the involvement of NRAMP1 and lipocalin-2, but not of hepcidin. Immunobiology. 2011;216(10):1127-34.

77. Ramboer E, Vanhaecke T, Rogiers V, Vinken M. Immortalized Human Hepatic Cell Lines for In Vitro Testing and Research Purposes. Methods Mol Biol. 2015;1250:53-76.

78. Brolen G, Sivertsson L, Bjorquist P, Eriksson G, Ek M, Semb H, et al. Hepatocyte-like cells derived from human embryonic stem cells specifically via definitive endoderm and a progenitor stage. J Biotechnol. 2010;145(3):284-94.

79. Duan Y, Catana A, Meng Y, Yamamoto N, He S, Gupta S, et al. Differentiation and enrichment of hepatocyte-like cells from human embryonic stem cells in vitro and in vivo. Stem Cells. 2007;25(12):3058-68.

80. Lavon N, Yanuka O, Benvenisty N. Differentiation and isolation of hepatic-like cells from human embryonic stem cells. Differentiation. 2004;72(5):230-8.

81. Richter M, Piwocka O, Musielak M, Piotrowski I, Suchorska WM, Trzeciak T. From Donor to the Lab: A Fascinating Journey of Primary Cell Lines. Front Cell Dev Biol. 2021;9:711381.

82. Berry MN. Metabolic Properties of Cells Isolated from Adult Mouse Liver. J Cell Biol. 1962;15(1):1-8.

83. Berry MN, Friend DS. High-yield preparation of isolated rat liver parenchymal cells: a biochemical and fine structural study. J Cell Biol. 1969;43(3):506-20.

84. Zhang Y, He Y, Bharadwaj S, Hammam N, Carnagey K, Myers R, et al. Tissue-specific extracellular matrix coatings for the promotion of cell proliferation and maintenance of cell phenotype. Biomaterials. 2009;30(23-24):4021-8.

85. Rajendran D, Hussain A, Yip D, Parekh A, Shrirao A, Cho CH. Long-term liver-specific functions of hepatocytes in electrospun chitosan nanofiber scaffolds coated with fibronectin. J Biomed Mater Res A. 2017;105(8):2119-28.

86. Dunn JC, Tompkins RG, Yarmush ML. Hepatocytes in collagen sandwich: evidence for transcriptional and translational regulation. J Cell Biol. 1992;116(4):1043-53.

87. Deharde D, Schneider C, Hiller T, Fischer N, Kegel V, Lubberstedt M, et al. Bile canaliculi formation and biliary transport in 3D sandwich-cultured hepatocytes in dependence of the extracellular matrix composition. Arch Toxicol. 2016;90(10):2497-511.

88. Chang TT, Hughes-Fulford M. Molecular mechanisms underlying the enhanced functions of three-dimensional hepatocyte aggregates. Biomaterials. 2014;35(7):2162-71.

89. Wong SF, No da Y, Choi YY, Kim DS, Chung BG, Lee SH. Concave microwell based size-controllable hepatosphere as a three-dimensional liver tissue model. Biomaterials. 2011;32(32):8087-96.

90. Rose S, Ezan F, Cuvellier M, Bruyere A, Legagneux V, Langouet S, et al. Generation of proliferating human adult hepatocytes using optimized 3D culture conditions. Sci Rep. 2021;11(1):515.

91. Messina A, Luce E, Hussein M, Dubart-Kupperschmitt A. Pluripotent-Stem-Cell-Derived Hepatic Cells: Hepatocytes and Organoids for Liver Therapy and Regeneration. Cells-Basel. 2020;9(2).

92. Pettinato G, Lehoux S, Ramanathan R, Salem MM, He LX, Muse O, et al. Generation of fully functional hepatocyte-like organoids from human induced pluripotent stem cells mixed with Endothelial Cells. Sci Rep. 2019;9(1):8920.

93. Peng WC, Kraaier LJ, Kluiver TA. Hepatocyte organoids and cell transplantation: What the future holds. Exp Mol Med. 2021;53(10):1512-28.

94. Guguenguillouzo C, Clement B, Baffet G, Beaumont C, Morelchany E, Glaise D, et al. Maintenance and Reversibility of Active Albumin Secretion by Adult-Rat Hepatocytes Co-Cultured with Another Liver Epithelial-Cell Type. Exp Cell Res. 1983;143(1):47-54.

95. Ghosh P, Sasaki K, Ruiz IAP, King KE, Weinman SA, Wozniak AL. Inflammatory macrophage to hepatocyte signals can be prevented by extracellular vesicle reprogramming. J Cell Sci. 2023;136(9).

96. Shoemaker JT, Zhang W, Atlas SI, Bryan RA, Inman SW, Vukasinovic J. A 3D Cell Culture Organ-on-a-Chip Platform With a Breathable Hemoglobin Analogue Augments and Extends Primary Human Hepatocyte Functions in vitro. Front Mol Biosci. 2020;7:568777.

97. Gomez-Lechon MJ, Donato MT, Castell JV, Jover R. Human hepatocytes as a tool for studying toxicity and drug metabolism. Curr Drug Metab. 2003;4(4):292-312.
98. MacDonald C. Development of new cell lines for animal cell biotechnology. Crit Rev Biotechnol. 1990;10(2):155-78.
99. Kaur G, Dufour JM. Cell lines: Valuable tools or useless artifacts. Spermatogenesis. 2012;2(1):1-5.
100. Gao GZ, Sun T. [Be vigilant against cross contamination of tumor cells in culture]. Zhonghua Nei Ke Za Zhi. 2013;52(9):715-7.
101. Capes-Davis A, Theodosopoulos G, Atkin I, Drexler HG, Kohara A, MacLeod RA, et al. Check your cultures! A list of cross-contaminated or misidentified cell lines. Int J Cancer. 2010;127(1):1-8.
102. Gerets HH, Tilmant K, Gerin B, Chanteux H, Depelchin BO, Dhalluin S, et al. Characterization of primary human hepatocytes, HepG2 cells, and HepaRG cells at the mRNA level and CYP activity in response to inducers and their predictivity for the detection of human hepatotoxins. Cell Biol Toxicol. 2012;28(2):69-87.
103. Serras AS, Rodrigues JS, Cipriano M, Rodrigues AV, Oliveira NG, Miranda JP. A Critical Perspective on 3D Liver Models for Drug Metabolism and Toxicology Studies. Front Cell Dev Biol. 2021;9:626805.
104. Tabernilla A, Dos Santos Rodrigues B, Pieters A, Caufriez A, Leroy K, Van Campenhout R, et al. In Vitro Liver Toxicity Testing of Chemicals: A Pragmatic Approach. Int J Mol Sci. 2021;22(9).
105. Castell JV, Jover R, Martinez-Jimenez CP, Gomez-Lechon MJ. Hepatocyte cell lines: their use, scope and limitations in drug metabolism studies. Expert Opin Drug Metab Toxicol. 2006;2(2):183-212.
106. Nagarajan SR, Paul-Heng M, Krycer JR, Fazakerley DJ, Sharland AF, Hoy AJ. Lipid and glucose metabolism in hepatocyte cell lines and primary mouse hepatocytes: a comprehensive resource for in vitro studies of hepatic metabolism. Am J Physiol Endocrinol Metab. 2019;316(4):E578-E89.
107. Clayton RF, Rinaldi A, Kandyba EE, Edward M, Willberg C, Klenerman P, et al. Liver cell lines for the study of hepatocyte functions and immunological response. Liver Int. 2005;25(2):389-402.
108. Chen B, Sirota M, Fan-Minogue H, Hadley D, Butte AJ. Relating hepatocellular carcinoma tumor samples and cell lines using gene expression data in translational research. BMC Med Genomics. 2015;8 Suppl 2(Suppl 2):S5.
109. Maqsood MI, Matin MM, Bahrami AR, Ghasroldasht MM. Immortality of cell lines: challenges and advantages of establishment. Cell Biol Int. 2013;37(10):1038-45.

110. Wu JC, Merlino G, Fausto N. Establishment and characterization of differentiated, nontransformed hepatocyte cell lines derived from mice transgenic for transforming growth factor alpha. Proc Natl Acad Sci U S A. 1994;91(2):674-8.

111. Hsiao PJ, Chiou HC, Jiang HJ, Lee MY, Hsieh TJ, Kuo KK. Pioglitazone Enhances Cytosolic Lipolysis, beta-oxidation and Autophagy to Ameliorate Hepatic Steatosis. Sci Rep. 2017;7(1):9030.

112. Guo L, Zhou SR, Wei XB, Liu Y, Chang XX, Liu Y, et al. Acetylation of Mitochondrial Trifunctional Protein alpha-Subunit Enhances Its Stability To Promote Fatty Acid Oxidation and Is Decreased in Nonalcoholic Fatty Liver Disease. Mol Cell Biol. 2016;36(20):2553-67.

113. Tao GZ, Lehwald N, Jang KY, Baek J, Xu B, Omary MB, et al. Wnt/beta-catenin signaling protects mouse liver against oxidative stress-induced apoptosis through the inhibition of forkhead transcription factor FoxO3. J Biol Chem. 2013;288(24):17214-24.

114. collection A-Abc. AML12 cells n.d [Available from: https://www.atcc.org/products/crl-2254.

115. Silva T, Moreira AC, Nazmi K, Moniz T, Vale N, Rangel M, et al. Lactoferricin Peptides Increase Macrophages' Capacity To Kill Mycobacterium avium. mSphere. 2017;2(4).

116. Fernandes SS, Nunes A, Gomes AR, de Castro B, Hider RC, Rangel M, et al. Identification of a new hexadentate iron chelator capable of restricting the intramacrophagic growth of Mycobacterium avium. Microbes Infect. 2010;12(4):287-94.

117. Glass CK, Natoli G. Molecular control of activation and priming in macrophages. Nat Immunol. 2016;17(1):26-33.

118. Murray PJ, Allen JE, Biswas SK, Fisher EA, Gilroy DW, Goerdt S, et al. Macrophage activation and polarization: nomenclature and experimental guidelines. Immunity. 2014;41(1):14-20.

119. Silva FSG, Starostina IG, Ivanova VV, Rizvanov AA, Oliveira PJ, Pereira SP. Determination of Metabolic Viability and Cell Mass Using a Tandem Resazurin/Sulforhodamine B Assay. Curr Protoc Toxicol. 2016;68:2 24 1-2 15.

120. Skehan P, Storeng R, Scudiero D, Monks A, McMahon J, Vistica D, et al. New colorimetric cytotoxicity assay for anticancer-drug screening. J Natl Cancer Inst. 1990;82(13):1107-12.

121. Papazisis KT, Geromichalos GD, Dimitriadis KA, Kortsaris AH. Optimization of the sulforhodamine B colorimetric assay. J Immunol Methods. 1997;208(2):151-8.

122. Vichai V, Kirtikara K. Sulforhodamine B colorimetric assay for cytotoxicity screening. Nat Protoc. 2006;1(3):1112-6.

123. O'Brien J, Wilson I, Orton T, Pognan F. Investigation of the Alamar Blue (resazurin) fluorescent dye for the assessment of mammalian cell cytotoxicity. Eur J Biochem. 2000;267(17):5421-6.
124. Voytik-Harbin SL, Brightman AO, Waisner B, Lamar CH, Badylak SF. Application and evaluation of the alamarBlue assay for cell growth and survival of fibroblasts. In Vitro Cell Dev Biol Anim. 1998;34(3):239-46.
125. Zumpe C, Bachmann CL, Metzger AU, Wiedemann N. Comparison of potency assays using different read-out systems and their suitability for quality control. J Immunol Methods. 2010;360(1-2):129-40.
126. Pace RT, Burg KJ. Toxic effects of resazurin on cell cultures. Cytotechnology. 2015;67(1):13-7.
127. Wu S, Yang J, Sun G, Hu J, Zhang Q, Cai J, et al. Macrophage extracellular traps aggravate iron overload-related liver ischaemia/reperfusion injury. Br J Pharmacol. 2021;178(18):3783-96.
128. Liu B, Deng X, Jiang Q, Li G, Zhang J, Zhang N, et al. Scoparone improves hepatic inflammation and autophagy in mice with nonalcoholic steatohepatitis by regulating the ROS/P38/Nrf2 axis and PI3K/AKT/mTOR pathway in macrophages. Biomed Pharmacother. 2020;125:109895.
129. Zhou K, Han J, Wang Y, Xu Y, Zhang Y, Zhu C. The therapeutic potential of bone marrow-derived macrophages in neurological diseases. CNS Neurosci Ther. 2022;28(12):1942-52.
130. Guc E, Brownlie D, Rodriguez-Tirado C, Kitamura T, Pollard JW. Generation of mouse bone marrow-derived macrophages using tumor coculture assays to mimic the tumor microenvironment. Methods Enzymol. 2020;632:91-111.
131. Silva T, Magalhaes B, Maia S, Gomes P, Nazmi K, Bolscher JG, et al. Killing of Mycobacterium avium by lactoferricin peptides: improved activity of arginine- and D-amino-acid-containing molecules. Antimicrob Agents Chemother. 2014;58(6):3461-7.
132. Galland F, Seady M, Taday J, Smaili SS, Goncalves CA, Leite MC. Astrocyte culture models: Molecular and function characterization of primary culture, immortalized astrocytes and C6 glioma cells. Neurochem Int. 2019;131:104538.
133. Gattermann N, Muckenthaler MU, Kulozik AE, Metzgeroth G, Hastka J. The Evaluation of Iron Deficiency and Iron Overload. Dtsch Arztebl Int. 2021;118(49):847-56.
134. Milic S, Mikolasevic I, Orlic L, Devcic E, Starcevic-Cizmarevic N, Stimac D, et al. The Role of Iron and Iron Overload in Chronic Liver Disease. Med Sci Monit. 2016;22:2144-51.

135. Messner DJ, Rhieu BH, Kowdley KV. Iron overload causes oxidative stress and impaired insulin signaling in AML-12 hepatocytes. Dig Dis Sci. 2013;58(7):1899-908.
136. Hirano S, Zhou Q, Furuyama A, Kanno S. Differential Regulation of IL-1beta and IL-6 Release in Murine Macrophages. Inflammation. 2017;40(6):1933-43.
137. Yeh KY, Yeh M, Glass J. Hepcidin regulation of ferroportin 1 expression in the liver and intestine of the rat. Am J Physiol Gastrointest Liver Physiol. 2004;286(3):G385-94.
138. Kim YJ, Park WR, Choi B, Choi HS, Kim DK. Epigallocatechin-3-Gallate Suppresses BMP-6-Mediated SMAD1/5/8 Transactivation of Hepcidin Gene by Inducing SMILE in Hepatocytes. Antioxidants (Basel). 2021;10(10).
139. Roetto A, Mezzanotte M, Pellegrino RM. The Functional Versatility of Transferrin Receptor 2 and Its Therapeutic Value. Pharmaceuticals (Basel). 2018;11(4).
140. Kawabata H, Germain RS, Ikezoe T, Tong X, Green EM, Gombart AF, et al. Regulation of expression of murine transferrin receptor 2. Blood. 2001;98(6):1949-54.
141. Kawabata H, Yang R, Hirama T, Vuong PT, Kawano S, Gombart AF, et al. Molecular cloning of transferrin receptor 2. A new member of the transferrin receptor-like family. J Biol Chem. 1999;274(30):20826-32.
142. Weis S, Carlos AR, Moita MR, Singh S, Blankenhaus B, Cardoso S, et al. Metabolic Adaptation Establishes Disease Tolerance to Sepsis. Cell. 2017;169(7):1263-+.

VI – Supplementary Information

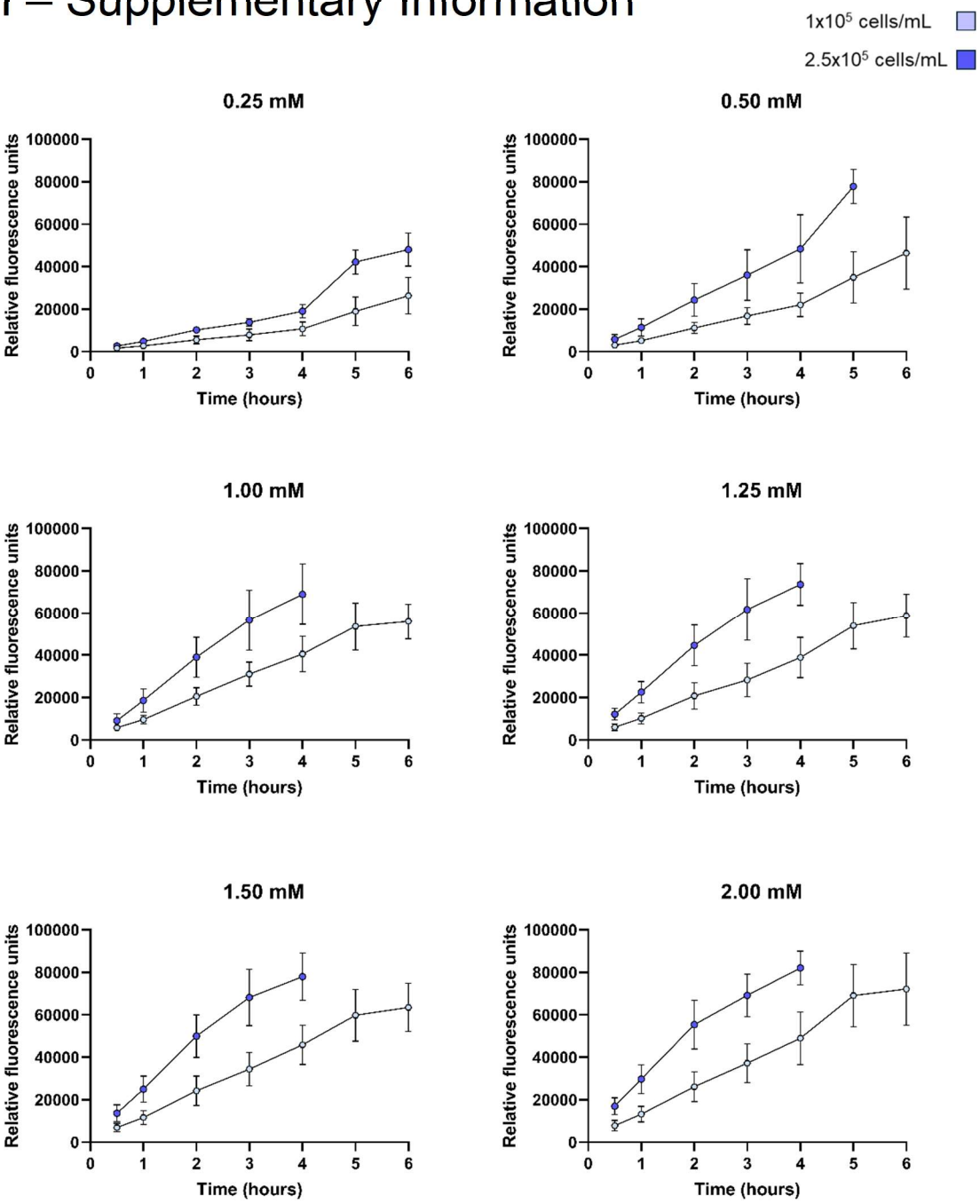

Figure S1. Graphical representation of the resazurin assay optimisation. Each resazurin concentration tested is depicted in a graph which compares the two cell densities ($1x10^5$ cells/mL in blue and $2.5x10^5$ cells/mL in dark blue) over time. Cells were kept for 6 hours after resazurin application, and for each of the time points indicated, the resorufin signal was measured. Data are expressed as the average ± SD of four independent experiments with triplicates. Statistics: ordinary one-way ANOVA.

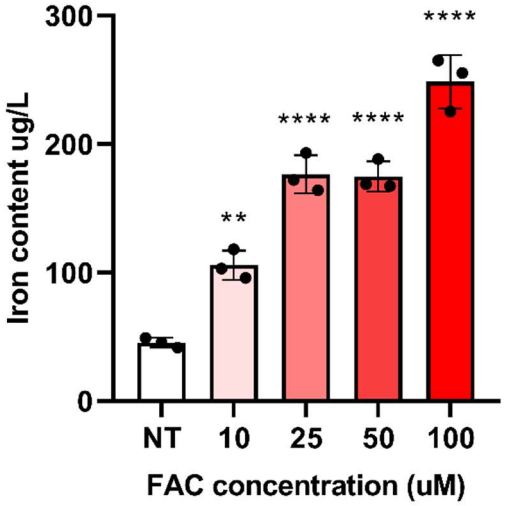

Figure S2. Graphical representation of AML12 iron content, in µg/L, in the presence of FAC in increasing concentrations (1, 10, 25, 50 and 100 µM). Cells were treated 24 hours after seeding and kept for another 48 hours afterwards. Iron content was determined through atomic absorption spectrometry. The graph represents the average ± SD of triplicates of one independent experiment. Statistics: ordinary one-way ANOVA.